Electronic Supplementary Information

5,20-Diheterohexaphyrins: metal-template-free synthesis and aromaticity switching

Masataka Umetani,[a] Jinseok Kim,[b] Takayuki Tanaka,*[a] Dongho Kim*[b] and Atsuhiro Osuka*[a]

[a]Department of Chemistry, Graduate School of Science, Kyoto University
[b]Spectroscopy Laboratory for Functional π-Electronic Systems and Department of Chemistry, Yonsei University

E-mail: taka@kuchem.kyoto-u.ac.jp
osuka@kuchem.kyoto-u.ac.jp
dongho@yonsei.ac.kr

Contents

1. Instrumentation and Materials

Commercially available solvents and reagents were used without further purification unless otherwise noted. The spectroscopic grade solvents were used as solvents for all spectroscopic studies. *n*-Hexane was dried in MS 4A. Silica gel column chromatography was performed on Wakogel C-200, C-300 and C-400. Thin-layer chromatography (TLC) was carried out on aluminum sheets coated with silica gel 60 F254 (Merck 5554). UV/Visible absorption spectra were recorded on Shimadzu UV-3600 spectrometers. ^{1}H and ^{13}C NMR spectra were recorded on a JEOL ECA-600 spectrometer (operating as 600 MHz for ^{1}H and 151 MHz for ^{13}C) using the residual solvent as the internal reference for ^{1}H (δ = 7.26 ppm in $CDCl_3$) and for ^{13}C (δ = 77.16 ppm in $CDCl_3$). High-resolution atmospheric-pressure-chemical-ionization time-of-flight mass-spectrometry (HR-APCI-TOF-MS) was recorded on a BRUKER micrOTOF model using negative mode. Single-crystal X-ray diffraction analysis data were collected at –180 °C with a Rigaku XtaLAB P200 by using graphite monochromated Cu-$K\alpha$ radiation (λ = 1.54187 Å). Single-crystal X-ray diffraction analysis data for **10a** were collected at 90 K on a Brucker APEX II X-Ray diffractometer equipped with a large area CCD detector by using graphite monochromated Mo-$K\alpha$ radiation (λ = 0.71073 Å). The structures were solved by direct method (SHELXS-2013/1 or SHELXT-2014/5) and refined by SHELXL-2014/7 program.[S1] Redox potentials were measured on an ALS electrochemical analyzer model 660. Microwave reactions were carried out with Anton Paar Monowave 400 apparatus.

2. Experimental Section

5,20-dithia-10,15,25,30-tetraphenylhexaphyrin (**8a**)

A mixture of **7a** (26.6 mg, 50 μmol) and Na_2S (4.1 mg, 53 μmol) in dry DMA (5 mL) was stirred at 50 ºC for 9 h under Ar. After quenching with water, the solution was extracted with ethyl acetate. The organic fraction was washed by water and dried with anhydrous Na_2SO_4. The solvent was evaporated to dryness. The crude product was purified by column chromatography on silica gel (C-400: dichloromethane). Recrystallization from dichloromethane/methanol gave **8a** (6.5 mg, 8.1 μmol, 32%) as black solids.

^{1}H NMR ($CDCl_3$, r.t.) δ (ppm): 14.78 (s, 2H, NH), 7.4–7.5 (m, 20H, Ph-H), 6.94 (d, J = 4.6 Hz, 4H, β-H), 6.91 (d, J = 4.6 Hz, 4H, β-H), and 6.23 (s, 4H, β-H).

^{13}C NMR ($CDCl_3$, r.t.) δ (ppm): 140.29, 136.56, 131.26, 129,23, 128.00, and 124.88. (Some signals were not observed because of poor solubility.)

UV/Vis/NIR (CH_2Cl_2): λ_{max} [nm] (ε [M^{-1} cm^{-1}]) = 338 (43000), 432 (90000), and 533 (68000).

HR MALDI-TOF-MS (positive): m/z calcd for $[C_{52}H_{35}N_6{}^{32}S_2]^+$: 807.19 [$M$ + H]$^+$; found: 807.24.

1-amino-5,10-diphenyl-14-bromotripyrrin (**9a**)

To a solution of **7a** (106.3 mg, 0.20 mmol) in THF (20 mL), ammonia solution (7N, in methanol, 20 mL) was added and the mixture was stirred at room temperature for 72 h under Ar. After quenching with water, the solution was extracted with ethyl acetate. The organic fraction was washed by water and dried with anhydrous Na_2SO_4. The solvent was evaporated to dryness. The crude product was purified by column chromatography on silica gel (C-400: dichloromethane/ethyl acetate = 100/3). Recrystallization from *n*-hexane gave **9a** (73.2 mg, 0.56 mmol, 78%) as black solids.

^{1}H NMR ($CDCl_3$, r.t.) δ (ppm): 14.33 (s, 1H, NH), 7.35–7.5 (m, 10H, Ar-H), 6.76 (d, J = 4.6 Hz, 1H, β-H), 6.67 (d, J = 4.6 Hz, 1H, β-H), 6.43 (d, J = 4.6 Hz, 1H, β-H), 6.27 (m, 2H, β-H), 6.06 (d, J = 4.1 Hz, 1H, β-H), and 5.61 (br, 2H, NH).

^{13}C NMR ($CDCl_3$, r.t.) δ (ppm): 168.62, 152.87, 147.73, 145.52, 143,50, 140.49, 138.98, 137.50, 137.05, 136.24, 135.56, 131.17, 131.09, 129.04, 128.06, 127.85, 127.71, 126.16, 125.65, 124.35, 121.32, and 118.08.

HR APCI-TOF-MS (positive): m/z calcd for $[C_{26}H_{20}N_4{}^{79}Br]^+$: 467.0866 [$M$ + H]$^+$; found: 467.0864.

5,20-diaza-10,15,25,30-tetraphenyl[28]hexaphyrin (**10a**)

Sodium hydride (60% dispersion in paraffin liquid, 21.6 mg, 0.54 mmol) was washed by dry *n*-hexane under Ar and dried under vacuum, to which were added **9a** (84.1 mg, 0.18 mmol) and THF (36 mL) and the mixture was refluxed for 48 h under Ar. After quenching with an aqueous NH_4Cl solution, the solution was extracted with ethyl acetate. The organic fraction was washed by water and dried with anhydrous Na_2SO_4. The solvent was evaporated to dryness. The crude product was purified by column chromatography on silica gel (C-400: dichloromethane/ethyl acetate = 100/3). Recrystallization from dichloromethane/methanol gave **10a** (25.8 mg, 33 μmol, 37%) as black solids.

^{1}H NMR ($CDCl_3$, r.t.) δ (ppm): 7.25–7.35 (m, 12H, Ph-H), 7.15–7.25 (m, 8H, Ph-H), 6.19 (d, J = 4.6 Hz, 4H, β-H), 5.99 (d, J = 4.6 Hz, 4H, β-H), and 5.43 (s, 4H, β-H).

^{1}H NMR ($CDCl_3$, –60 ºC) δ (ppm): 19.96 (s, 1H, NH), 13.76 (s, 1H, NH), 7.25–7.35 (m, 12H, Ph-H), 7.15–

7.25 (m, 8H, Ph-H), 6.24 (br, 2H, β-H), 6.15 (br, 2H, β-H), 6.05 (br, 2H, β-H), 5.87 (br, 2H, β-H), 5.47 (br, 2H, β-H), and 5.39 (s, 2H, β-H). (Some signals assignable to NH protons were not observed presumably because of their broadness or tautomerism.)

^{13}C NMR ($CDCl_3$, r.t.) δ (ppm): 165.70, 139.83, 136.38, 130.11, 128.65, 128.05, 119.37, and 118.00. (Some signals were not observed because of poor solubility.)

UV/Vis/NIR (CH_2Cl_2): λ_{max} [nm] (ε [M^{-1} cm^{-1}]) = 312 (27000), 458 (100000) and 511 (68000).

HR APCI-TOF-MS (negative): *m*/*z* calcd for $[C_{52}H_{36}N_8]^-$: 772.3068 [*M*]$^-$; found: 772.3055.

5,20-diaza-10,15,25,30-tetraphenyl[26]hexaphyrin (11a)

To a solution of **10a** in dry CH_2Cl_2 and dry pyridine (1 drop), excess amount of PbO_2 was added and the mixture was stirred at room temperature for 30 seconds. The reaction mixture was quickly filtered through membrane filter.

The product is unstable in ambient conditions and used in the measurement immediately.

^{1}H NMR ($CDCl_3$, r.t.) δ (ppm): 8.77 (d, *J* = 4.6 Hz, 4H, β-H), 8.60 (s, 4H, β-H), 8.49 (d, *J* = 4.6 Hz, 4H, β-H), 8.17 (m, 8H, Ph-H), and 7.78 (m, 12H, Ph-H). (The signal assignable to NH protons was not observed presumably because of their broadness.)

UV/Vis/NIR (CH_2Cl_2/pyridine): λ_{max} [nm] = 591, 772, 919, and 1010.

1,14-dibromo-5,10-dimesityltripyrrin (7b)

A solution of 5,10-dimesityltripyrrane (554.0 mg, 1.20 mmol) in dry THF (24 mL) under Ar was cooled to –78 °C, to which *N*-bromosuccinimide (436.6 mg, 2.46 mmol) was added in two portions over 2.5 h. The reaction was quenched at –78 °C with an aqueous $Na_2S_2O_3$ solution. Dichloromethane was added and the organic layer was separated. The organic extract was washed by water and dried with anhydrous Na_2SO_4. The solvent was evaporated to dryness under a light-shielded condition. The crude product was filtered through silica gel (C-300: *n*-hexane/dichloromethane = 1/1) and the filtrate was concentrated under reduced pressure under a light-shielded condition. The product was dissolved in dry dichloromethane (120 mL) under Ar and cooled to 0 °C. DDQ (544 g, 2.40 mmol) was added and the reaction mixture was stirred at 0 °C for 5 min. The reaction mixture was filtered through a short pad of alumina with dichloromethane as an eluent and the filtrate was concentrated under reduced pressure. The crude product was purified by column chromatography on silica gel (C-400: dichloromethane/n-hexane = 1/3) to give **7b** (508.6 mg, 0.826 mmol, 69%) as brown solids.

The product is unstable in ambient conditions and used in the next step immediately.

^{1}H NMR ($CDCl_3$, r.t.) δ (ppm): 13.63 (s, 1H, NH), 6.90 (s, 4H, Mes-H), 6.51 (d, *J* = 4.6 Hz, 2H, β-H), 6.44 (d, *J* = 4.1 Hz, 2H, β-H), 5.99 (br, 2H, β-H), 2.33 (s, 6H, Me-H), and 2.09 (s, 12H, Me-H).

^{13}C NMR ($CDCl_3$, r.t.) δ (ppm): 150.95, 150.46, 138.78, 138.07, 137.19, 137.03, 135.81, 132.56, 129.12, 128.09, 121.56, 21.24, and 20.20.

HR APCI-TOF-MS (positive): *m*/*z* calcd for $[C_{32}H_{30}N_3{}^{79}Br_2]^+$: 614.0801 [*M* + H]$^+$; found: 614.0797.

5,20-dithia-10,15,25,30-tetramesitylhexaphyrin (8b)

A mixture of **7b** (133.5 mg, 0.22 mmol) and Na_2S (16.9 mg, 0.22 mmol) in dry DMA (22 mL) was stirred

at 50 ºC for 18 h under Ar. After quenching with water, the solution was extracted with ethyl acetate. The organic fraction was washed by water and dried with anhydrous Na_2SO_4. The solvent was evaporated to dryness. The crude product was purified by column chromatography on silica gel (C-400: dichloromethane/*n*-hexane = 1/1). Recrystallization from dichloromethane/methanol gave **8b** (17.4 mg, 18 μmol, 16%) as black solids.

^{1}H NMR ($CDCl_3$, r.t.) δ (ppm): 15.10 (s, 2H, NH), 6.90 (s, 8H, Mes-H), 6.78 (d, J = 4.6 Hz, 4H, β-H), 6.63 (d, J = 4.6 Hz, 4H, β-H), 5.83 (d, J = 2.3 Hz, 4H, β-H), 2.33 (s, 12H, Me-H), and 2.14 (s, 24H, Me-H).

^{13}C NMR ($CDCl_3$, r.t.) δ (ppm): 164.84, 151.91, 139.95, 137.81, 137.28, 136.15, 135.23, 132.98, 128.06, 124.57, 121.04, 21.25, and 20.36.

UV/Vis/NIR (CH_2Cl_2): λ_{max} [nm] (ε [M^{-1} cm^{-1}]) = 335 (30000), 425 (76000), and 536 (59000).

HR APCI-TOF-MS (positive): *m*/*z* calcd for $[C_{64}H_{59}N_6{}^{32}S_2]^+$: 975.4237 [$M$ + H]$^+$; found: 975.4262.

1-amino-5,10-dimesityl-14-bromotripyrrin (**9b**)

To a solution of **7b** (375.1 mg, 0.61 mmol) in THF (30 mL), ammonia solution (7N, in methanol, 30 mL) was added and the mixture was stirred at room temperature for 72 h under Ar. After quenching with water, the solution was extracted with ethyl acetate. The organic fraction was washed by water and dried with anhydrous Na_2SO_4. The solvent was evaporated to dryness. The crude product was purified by column chromatography on silica gel (C-400: dichloromethane/ethyl acetate = 100/3). Recrystallization from *n*-hexane gave **9b** (219.4 mg, 0.40 mmol, 65%) as black solids.

^{1}H NMR ($CDCl_3$, r.t.) δ (ppm): 14.41 (s, 1H, NH), 6.89 (s, 2H, Mes-H), 6.88 (s, 2H, Mes-H), 6.53 (d, J = 4.6 Hz, 1H, β-H), 6.46 (d, J = 4.1 Hz, 1H, β-H), 6.34 (d, J = 4.6 Hz, 1H, β-H), 6.19 (d, J = 4.6 Hz, 1H, β-H), 6.00 (d, J = 3.7 Hz, 1H, β-H), 5.73 (brs, 1H, β-H), 5.68 (br, 2H, NH), 2.33 (s, 3H, Me-H), 2.32 (s, 3H, Me-H), 2.10 (s, 6H, Me-H), and 2.09 (s, 6H, Me-H).

^{13}C NMR ($CDCl_3$, r.t.) δ (ppm): 168.59, 152.82, 147.66, 145.35, 142.80, 139.41, 137.97, 137.90, 137.69, 137.29, 137.13, 134.95, 134.86, 133.27, 133.04, 127.97, 127.89, 125.59, 124.34, 123.15, 121.45, 116.95, 21.23, 20.43, and 20.14. (A signal was not observed presumably because of their broadness or overlapping.)

HR APCI-TOF-MS (positive): *m*/*z* calcd for $[C_{32}H_{32}N_4{}^{79}Br]^+$: 551.1805 [$M$ + H]$^+$; found: 551.1814.

5,20-diaza-10,15,25,30-tetramesityl[28]hexaphyrin (**10b**)

Sodium hydride (60% dispersion in paraffin liquid, 8.0 mg, 0.2 mmol) was washed by dry *n*-hexane under Ar and dried under vacuum, to which were added **9b** (55.2 mg, 0.10 mmol) and THF (20 mL) and the mixture was stirred at 200 ºC for 30 min under microwave irradiation. After quenching with an aqueous NH_4Cl solution, the solution was extracted with ethyl acetate. The organic fraction was washed by water and dried with anhydrous Na_2SO_4. The solvent was evaporated to dryness. The crude product was purified by column chromatography on silica gel (C-400: dichloromethane/ethyl acetate = 100/1). Recrystallization from dichloromethane/methanol gave **10b** (3.4 mg, 3.6 μmol, 7.2%) as black solids.

^{1}H NMR ($CDCl_3$, r.t.) δ (ppm): 6.80 (s, 8H, Mes-H), 5.92 (d, J = 4.6 Hz, 4H, β-H), 5.90 (br, 4H, β-H), 5.12 (s, 4H, β-H), 2.24 (s, 12H, Me-H), and 2.19 (s, 24H, Me-H).

^{1}H NMR ($CDCl_3$, –60 ºC) δ (ppm): 19.96 (s, 1H, NH), 18.34 (br, 1H, NH), 13.74 (br, 1H, NH), 13.54 (br, 1H, NH), 6.78 (m, 8H, Mes-H), 5.93 (br, 2H, β-H), 5.85 (br, 4H, β-H), 5.6–5.9 (br, 2H, β-H), 5.0–5.2 (br,

2H, β-H), 5.00 (br, 2H, β-H), 2.22 (s, 12H, Me-H), and 2.16 (s, 24H, Me-H).
^{13}C NMR ($CDCl_3$, r.t.) δ (ppm): 139.27, 137.36, 135.57, 132.16, 128.04, 118.21, 117.59, 21.18, and 20.04. (Some signals were not observed because of poor solubility.)
UV/Vis/NIR (CH_2Cl_2): λ_{max} [nm] (ε [M^{-1} cm^{-1}]) = 318 (27000), 446 (92000), and 512 (71000).
HR APCI-TOF-MS (negative): *m*/*z* calcd for $[C_{64}H_{60}N_8]^{-}$: 940.4946 [*M*]$^{-}$; found: 940.4942.

5,20-diaza-10,15,25,30-tetramesityl[26]hexaphyrin (**11b**)
To a solution of **10b** in dry CH_2Cl_2 and dry pyridine (1 drop), excess amount of PbO_2 was added and the mixture was stirred at room temperature for 30 seconds. The reaction mixture was quickly filtered through membrane filter.
The product is unstable under ambient conditions and was used in the measurement immediately.
^{1}H NMR ($CDCl_3$, r.t.) δ (ppm): 8.78 (d, J = 3.7 Hz, 4H, β-H), 8.31 (s, 4H, β-H), 8.29 (d, J = 4.6 Hz, 4H, β-H), 7.26 (s, 8H, Mes-H), 2.59 (s, 12H, Me-H), and 2.04 (s, 24H, Ph-H). (The signal assignable to NH protons was not observed presumably because of their broadness.)
^{1}H NMR ($CDCl_3$, –60 ºC) δ (ppm): 8.80 (d, J = 1.8 Hz, 4H, β-H), 8.36 (s, 4H, β-H), 8.34 (d, J = 2.1 Hz, 4H, β-H), 7.25 (s, 8H, Mes-H), 2.58 (s, 12H, Me-H), and 2.01 (s, 24H, Ph-H). (The signal assignable to NH protons was not observed presumably because of their broadness.)
UV/Vis/NIR (CH_2Cl_2/pyridine): λ_{max} [nm] = 586, 764, 918, and 1000.
Fluorescence (CH_2Cl_2/pyridine): λ_{ex} [nm] = 1027.

3. NMR Spectra

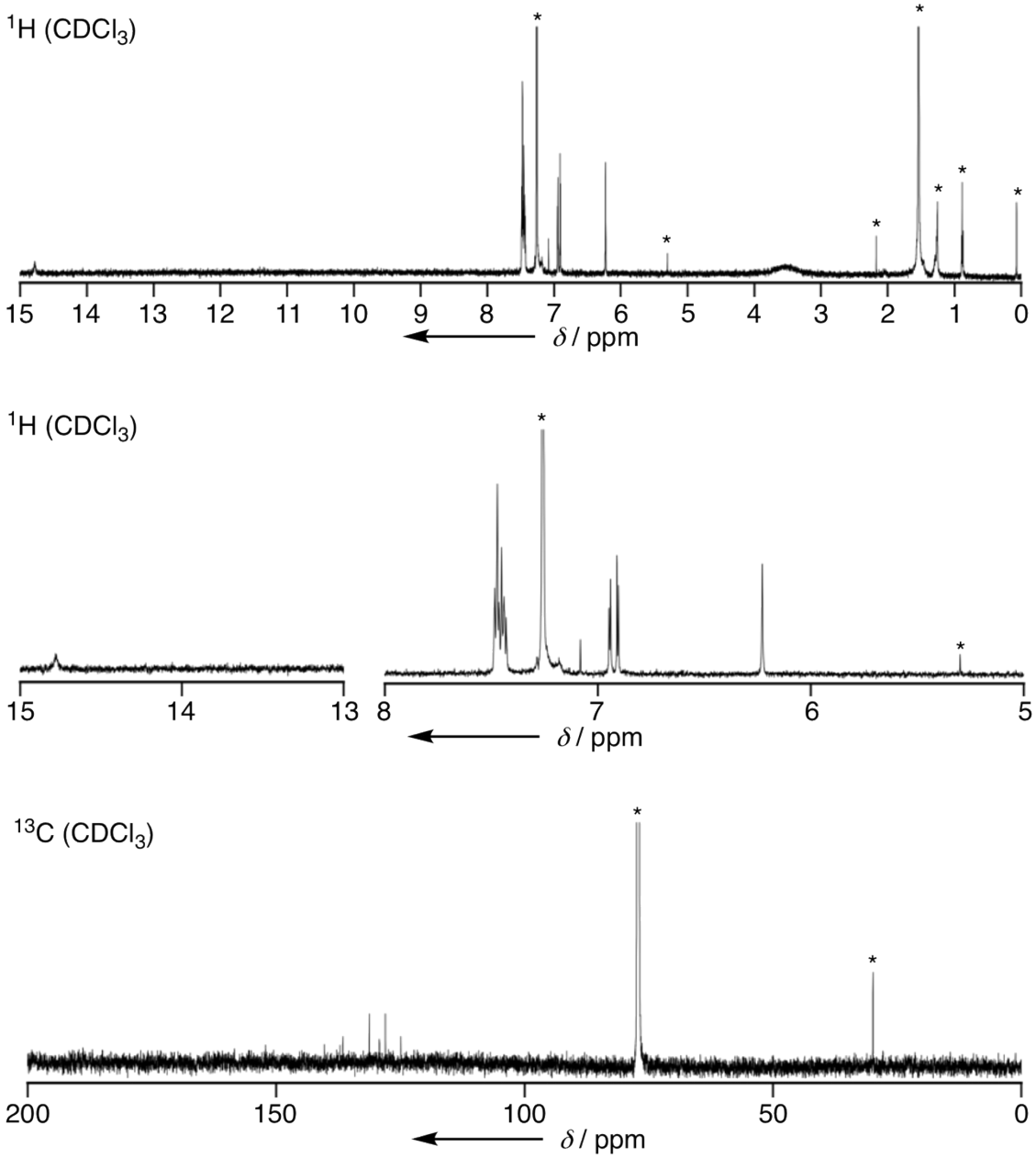

Figure S3-1-1. ^{1}H and ^{13}C NMR spectra of **8a** in $CDCl_3$ at room temperature. * means residual solvent peaks.

Some signals in ^{13}C NMR spectrum were not observed because of poor solubility.

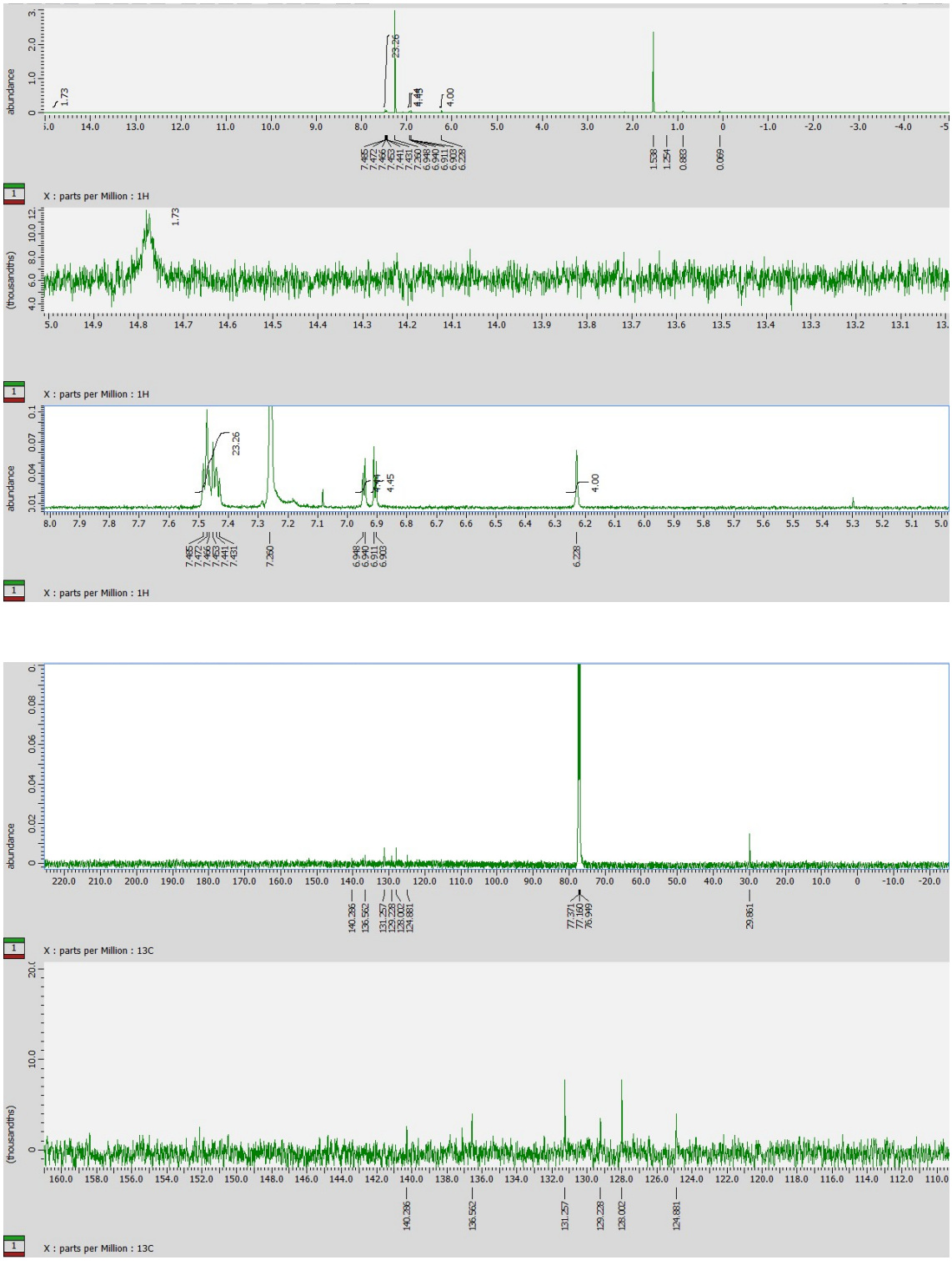

Figure S3-1-2. ^{1}H and ^{13}C NMR spectra of **8a** in $CDCl_3$ at room temperature.

Some signals in ^{13}C NMR spectrum were not observed because of poor solubility.

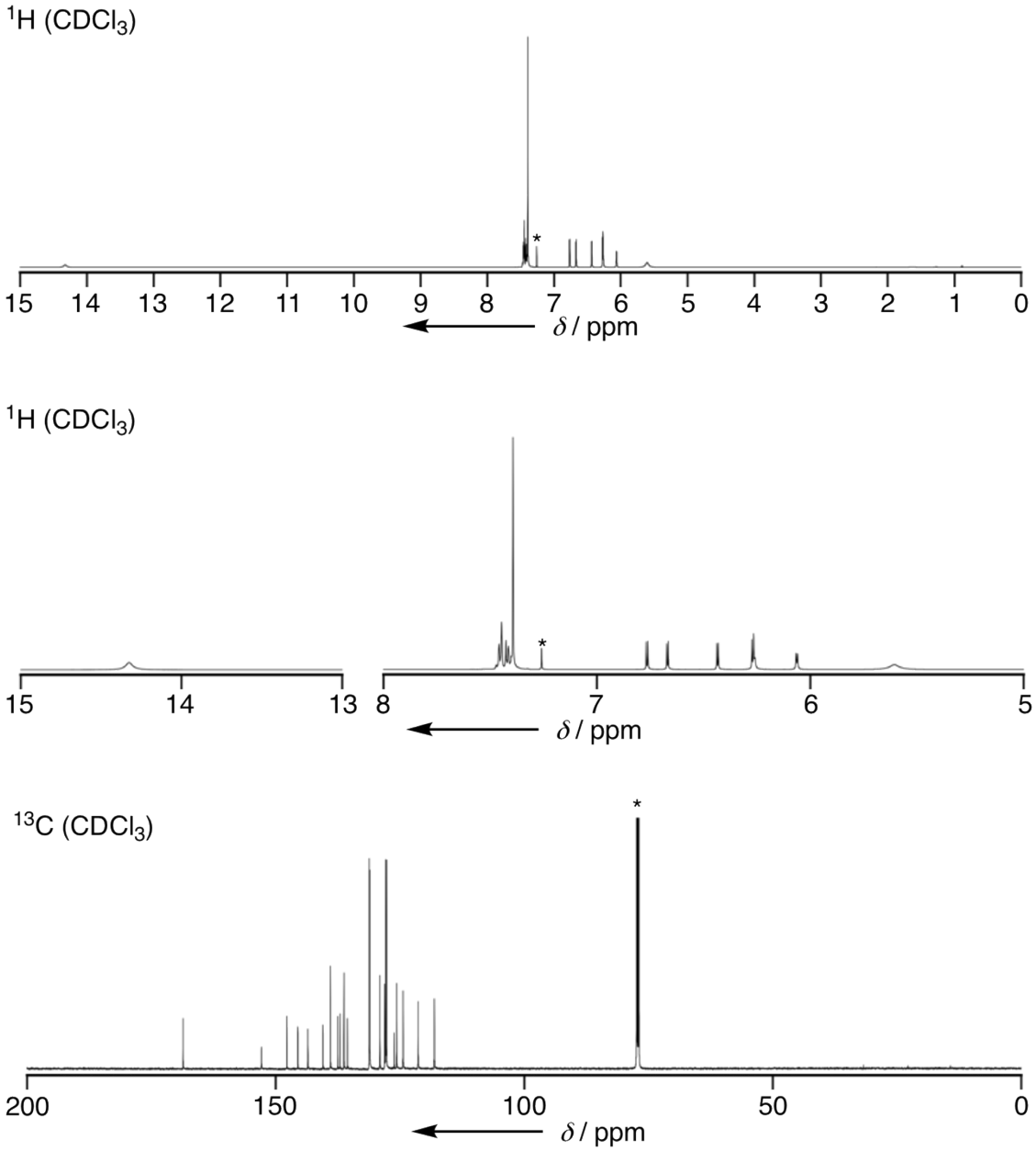

Figure S3-2-1. ^{1}H NMR spectra of **9a** in $CDCl_3$ at room temperature. * means residual solvent peaks.

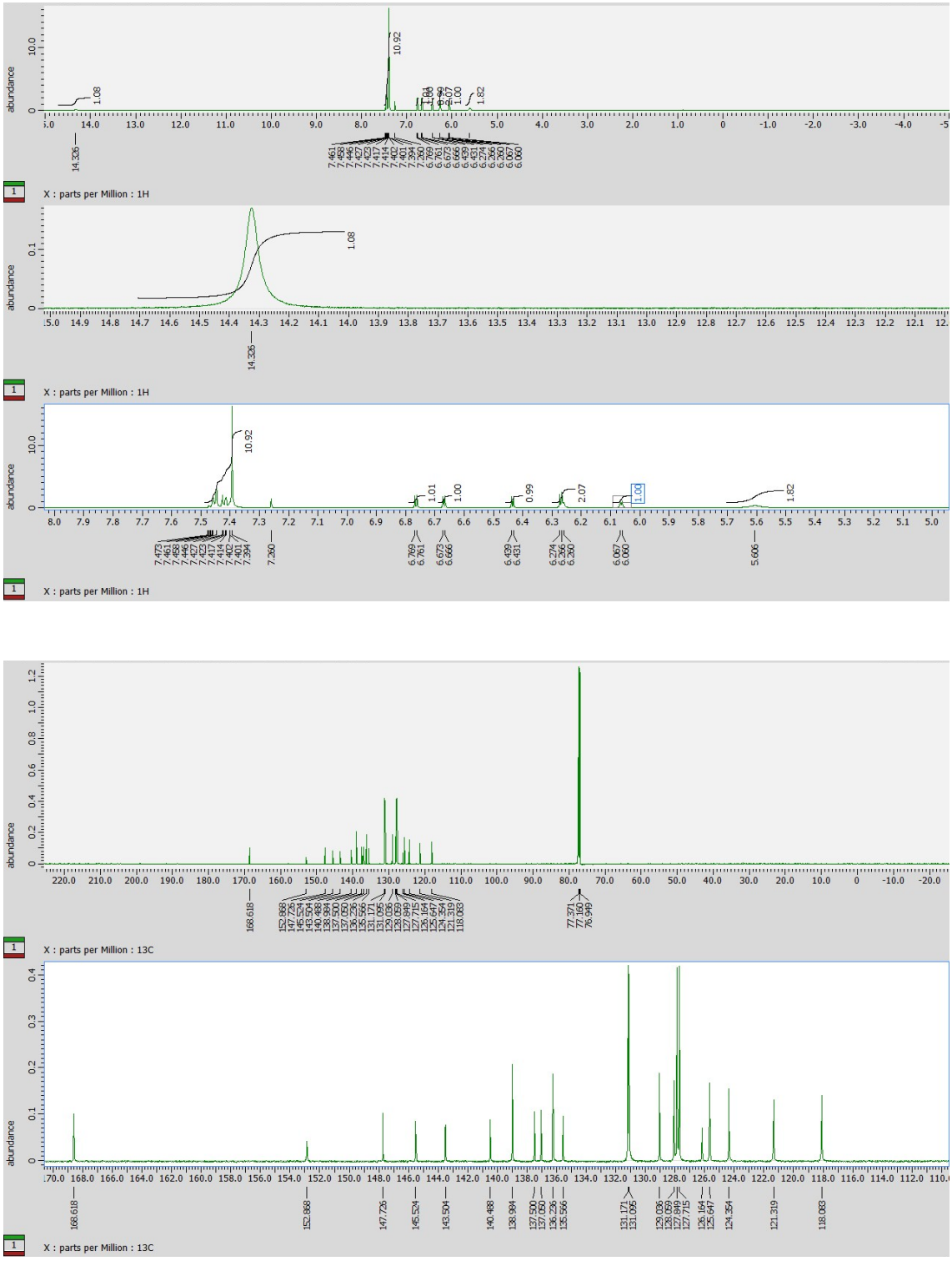

Figure S3-2-2. ^{1}H NMR spectra of **9a** in $CDCl_3$ at room temperature.

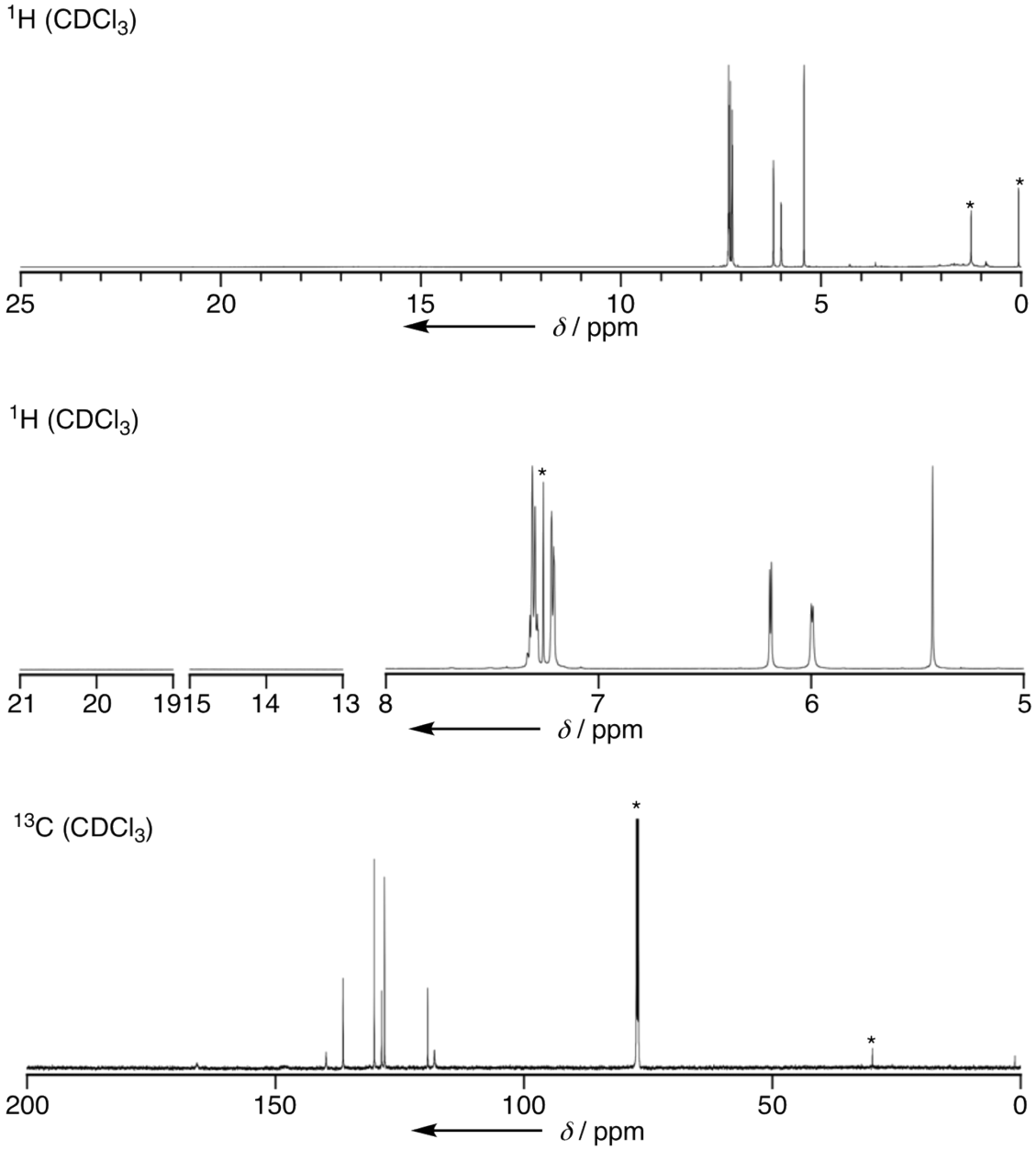

Figure S3-3-1. ^{1}H and ^{13}C NMR spectra of **10a** in $CDCl_3$ at room temperature. * means residual solvent peaks.

Some signals in ^{13}C NMR spectrum were not observed because of poor solubility.

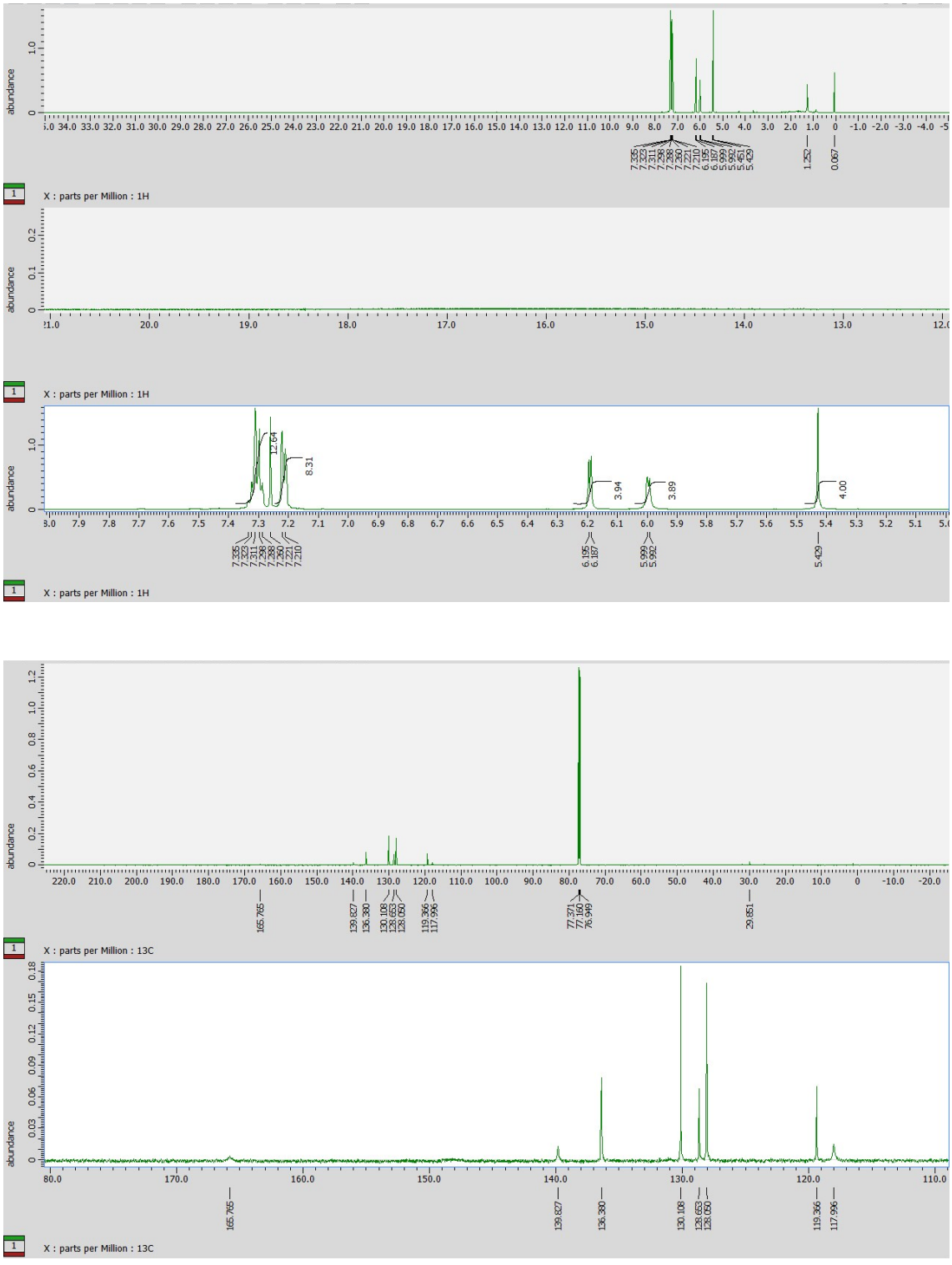

Figure S3-3-2. ^{1}H and ^{13}C NMR spectra of **10a** in $CDCl_3$ at room temperature.

Some signals in ^{13}C NMR spectrum were not observed because of poor solubility.

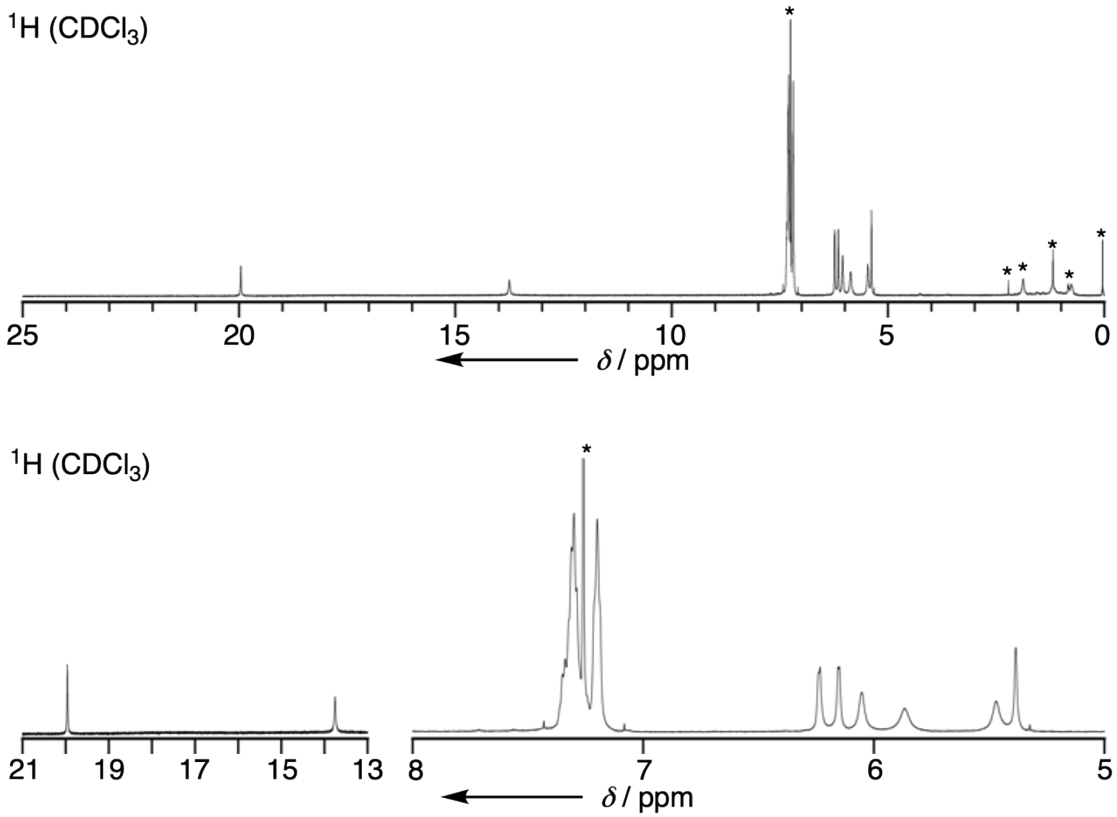

Figure S3-4-1. ^{1}H NMR spectra of **10a** in $CDCl_3$ at –60 ºC. * means residual solvent peaks.
Some signals assignable to NH protons were not observed presumably because of their broadness or tautomerism.

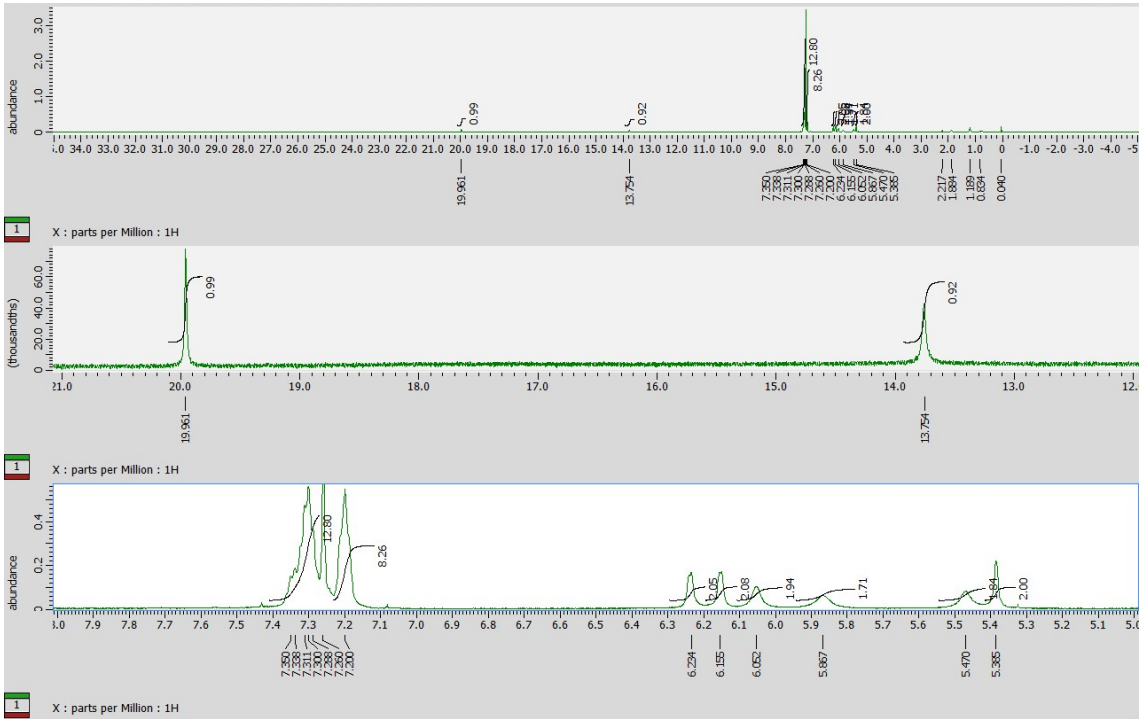

Figure S3-4-2. ^{1}H NMR spectra of **10a** in $CDCl_3$ at –60 ºC.

Some signals assignable to NH protons were not observed presumably because of their broadness or tautomerism.

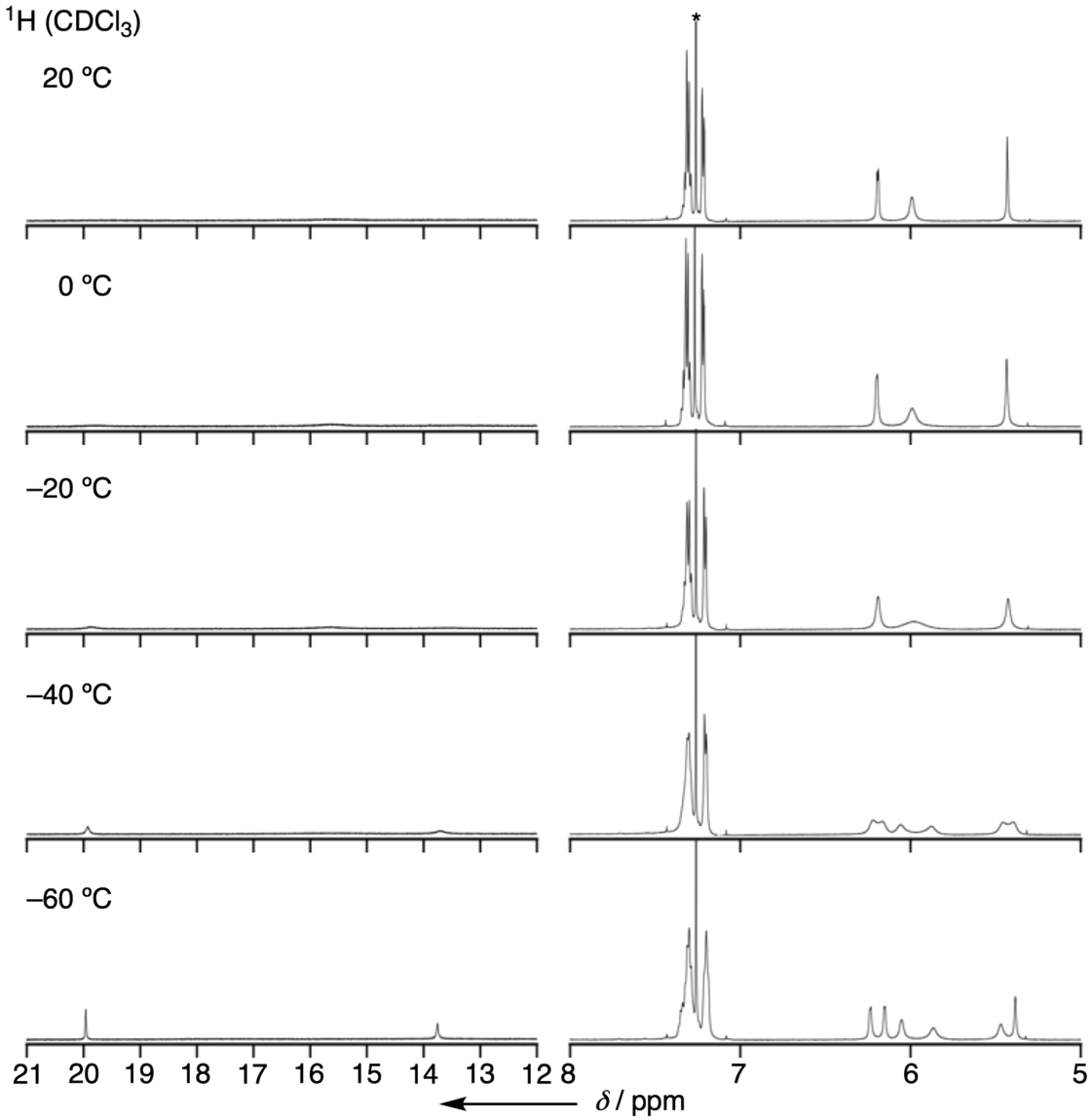

Figure S3-5. Variable temperature ^{1}H NMR spectra of **10a** in $CDCl_3$. * means residual solvent peaks.

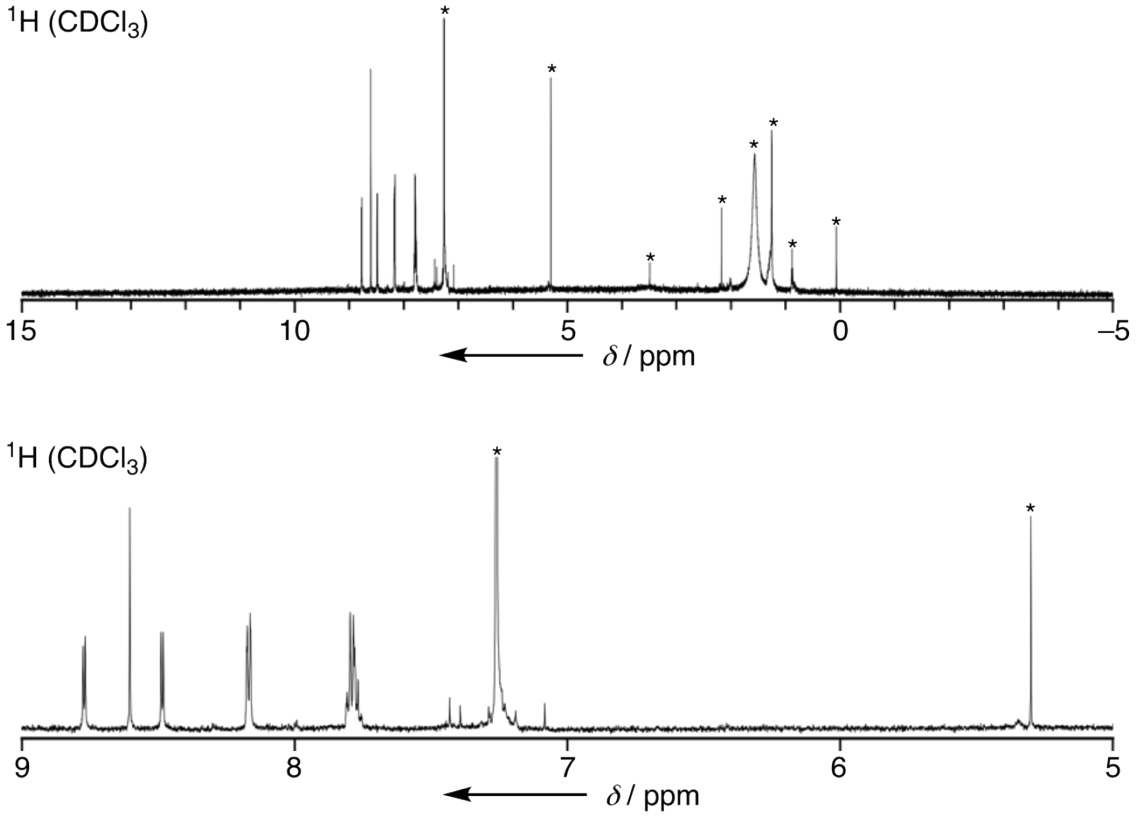

Figure S3-6-1. ^{1}H NMR spectra of **11a** in $CDCl_3$ at room temperature. * means residual solvent and impurity peaks.

The signal assignable to NH protons was not observed presumably because of their broadness.

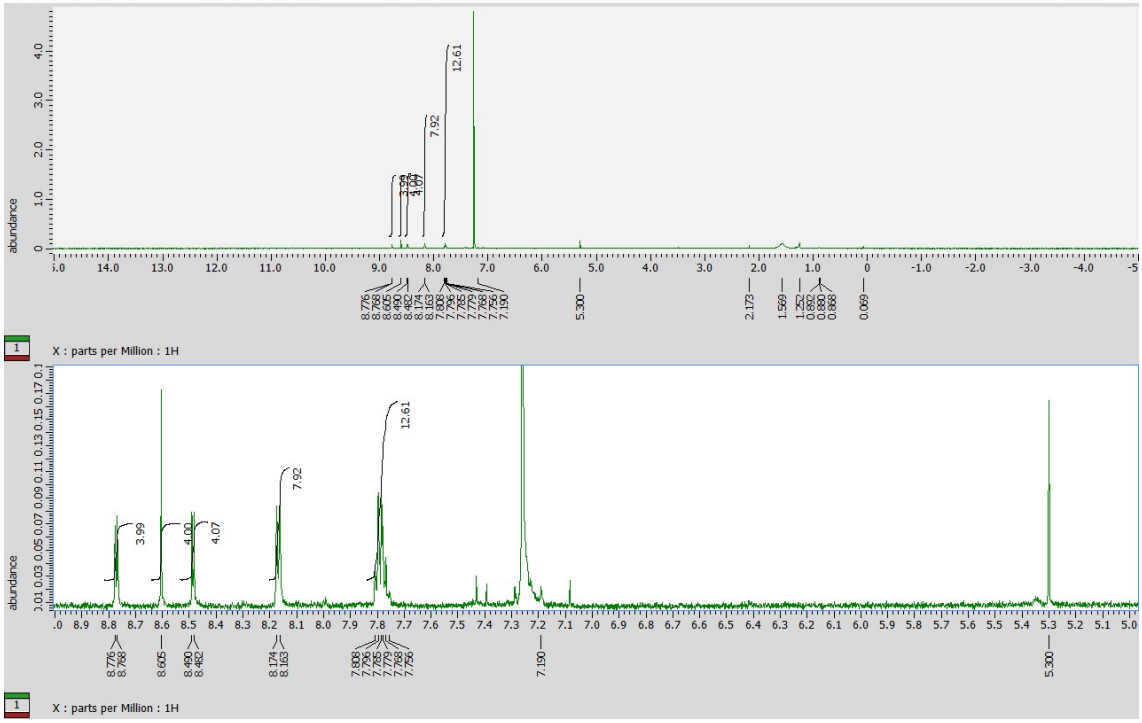

Figure S3-6-2. ^{1}H NMR spectra of **11a** in $CDCl_3$ at room temperature.

The signal assignable to NH protons was not observed presumably because of their broadness.

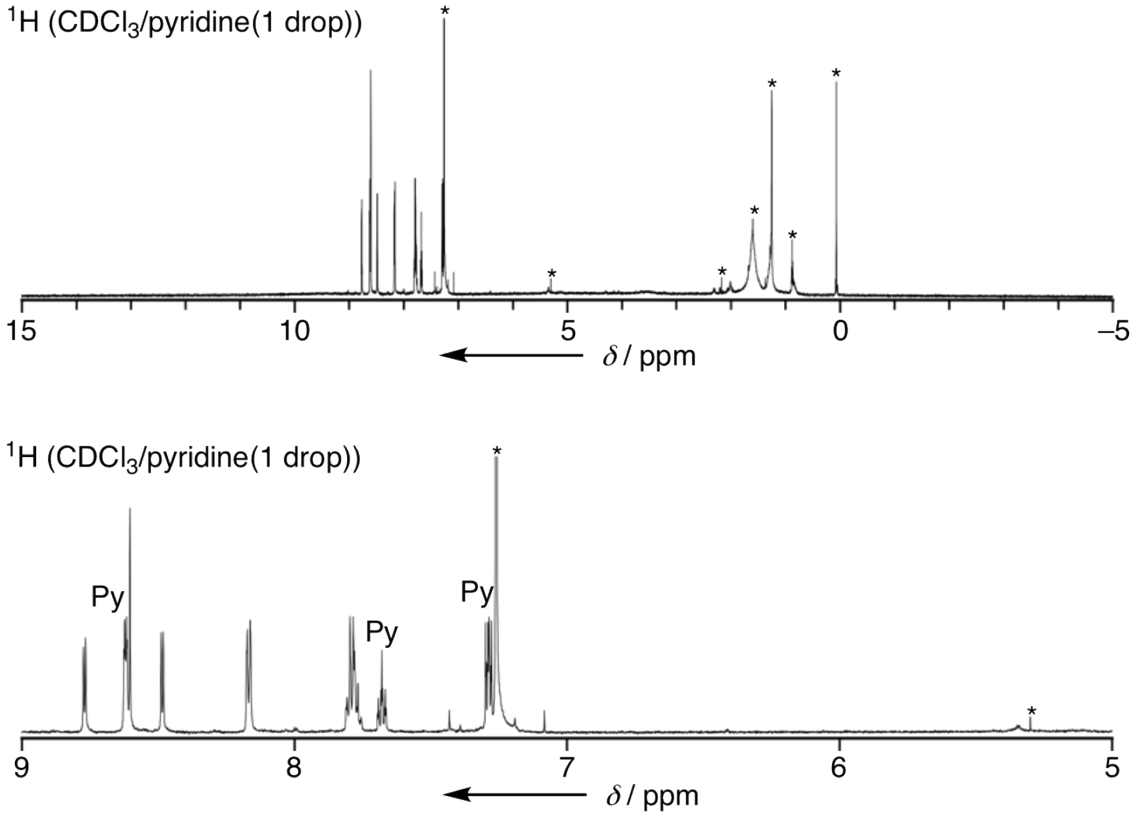

Figure S3-7-1. ^{1}H NMR spectra of **11a** in $CDCl_3$/pyridine (1 drop) at room temperature. * means residual solvent and impurity peaks.

The signal assignable to NH protons was not observed presumably because of their broadness.

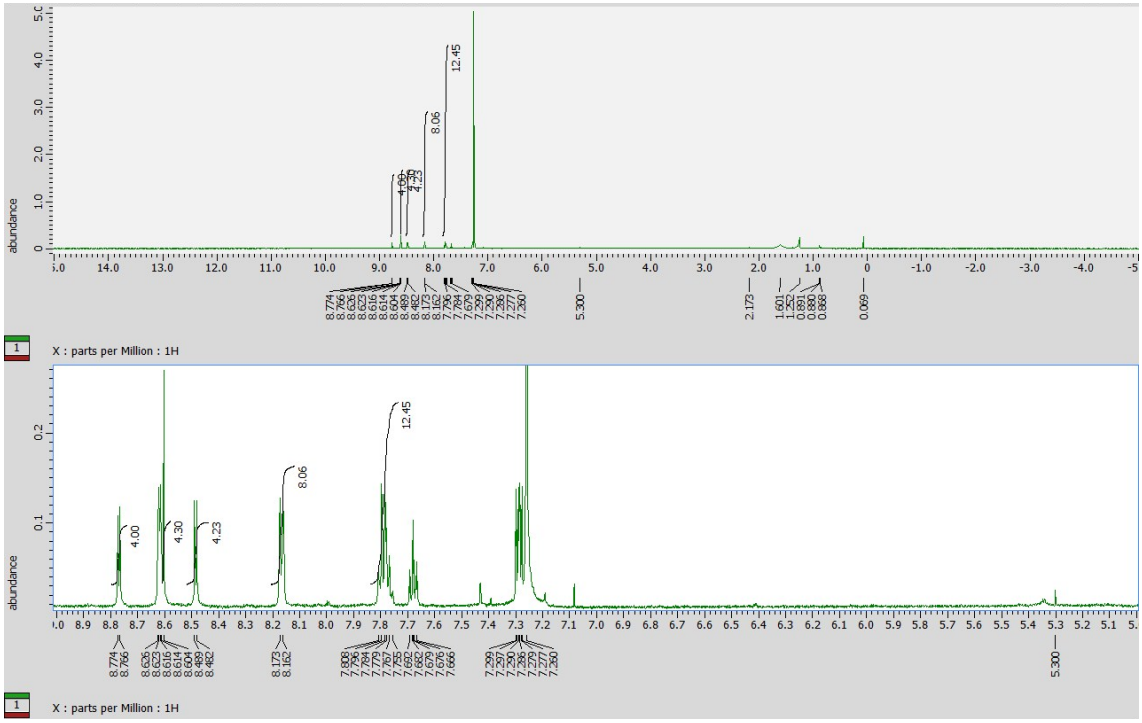

Figure S3-7-2. ^{1}H NMR spectra of **11a** in $CDCl_3$/pyridine (1 drop) at room temperature.
The signal assignable to NH protons was not observed presumably because of their broadness.

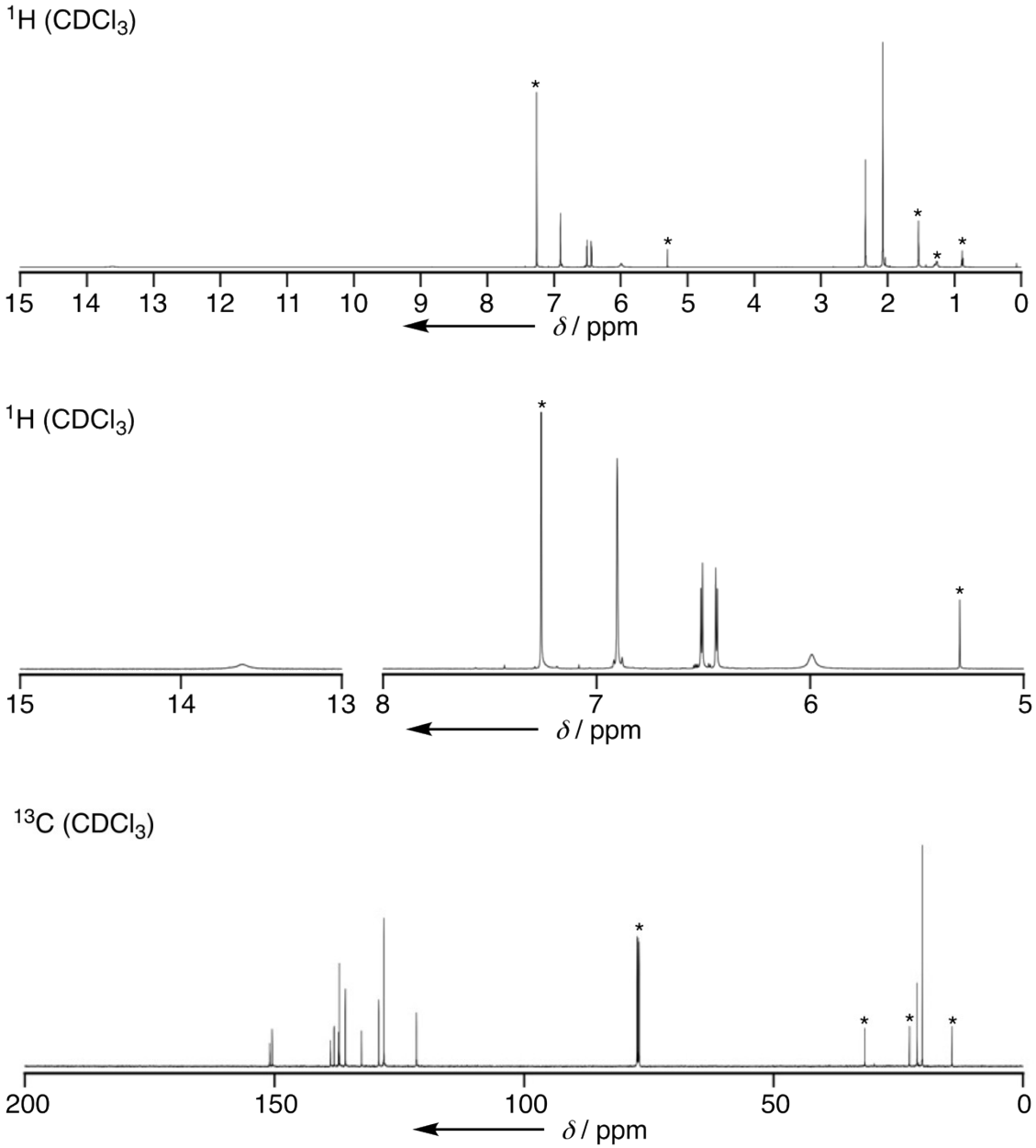

Figure S3-8-1. ^{1}H and ^{13}C NMR spectra of **7b** in $CDCl_3$ at room temperature. * means residual solvent and impurity peaks.

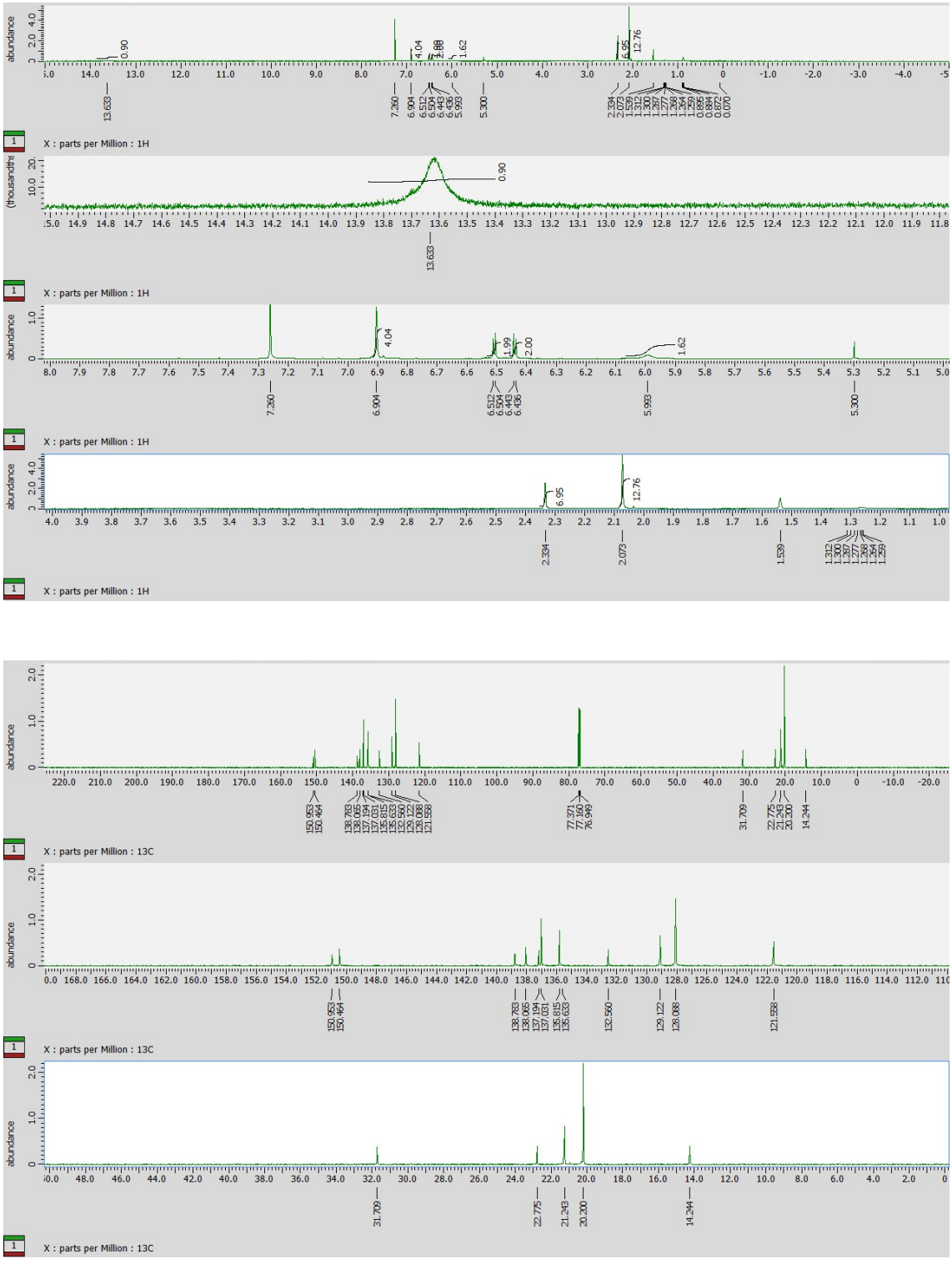

Figure S3-8-2. ^{1}H and ^{13}C NMR spectra of **7b** in $CDCl_3$ at room temperature.

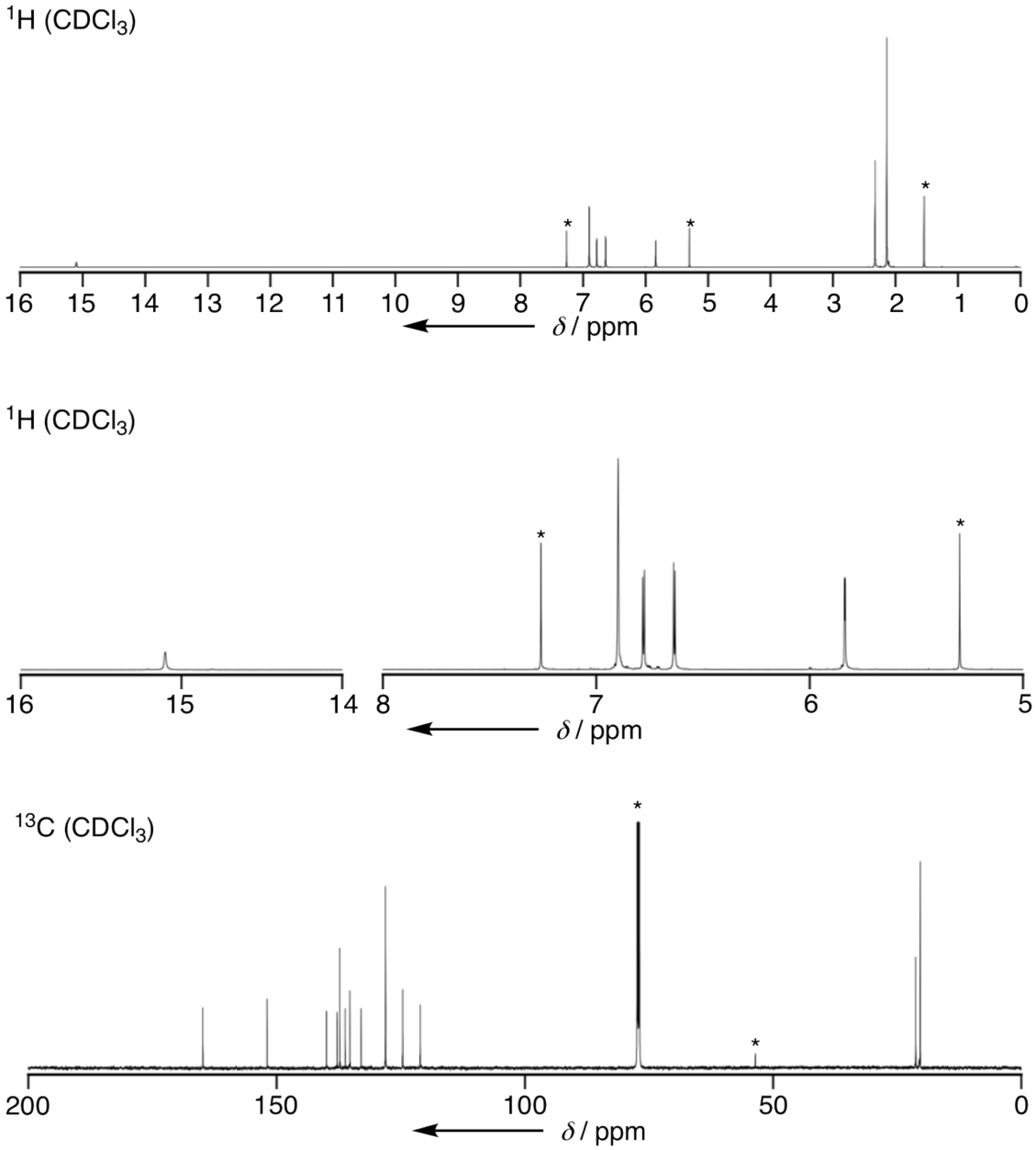

Figure S3-9-1. ^{1}H and ^{13}C NMR spectra of **8b** in $CDCl_3$ at room temperature. * means residual solvent and impurity peaks.

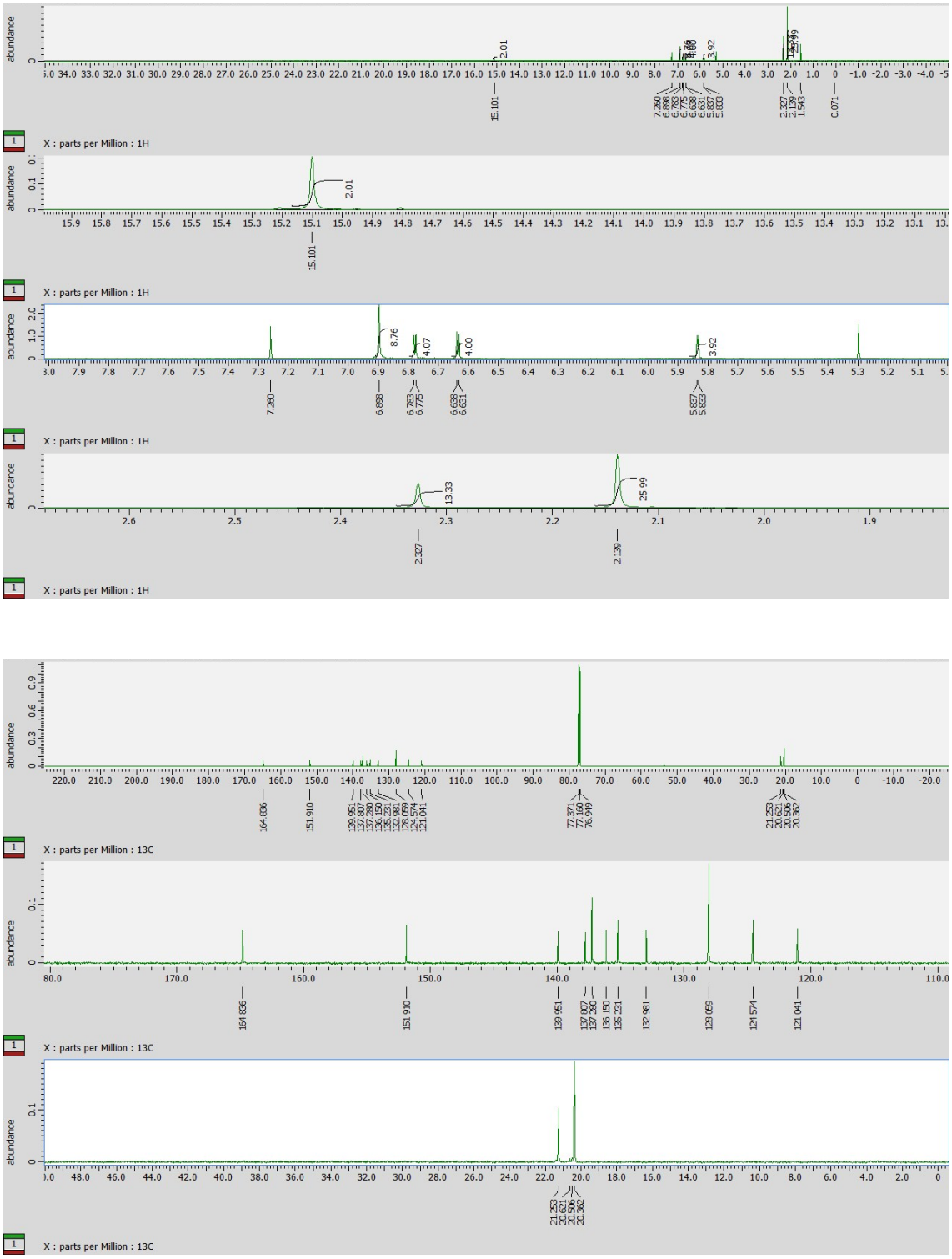

Figure S3-9-2. ^{1}H and ^{13}C NMR spectra of **8b** in $CDCl_3$ at room temperature.

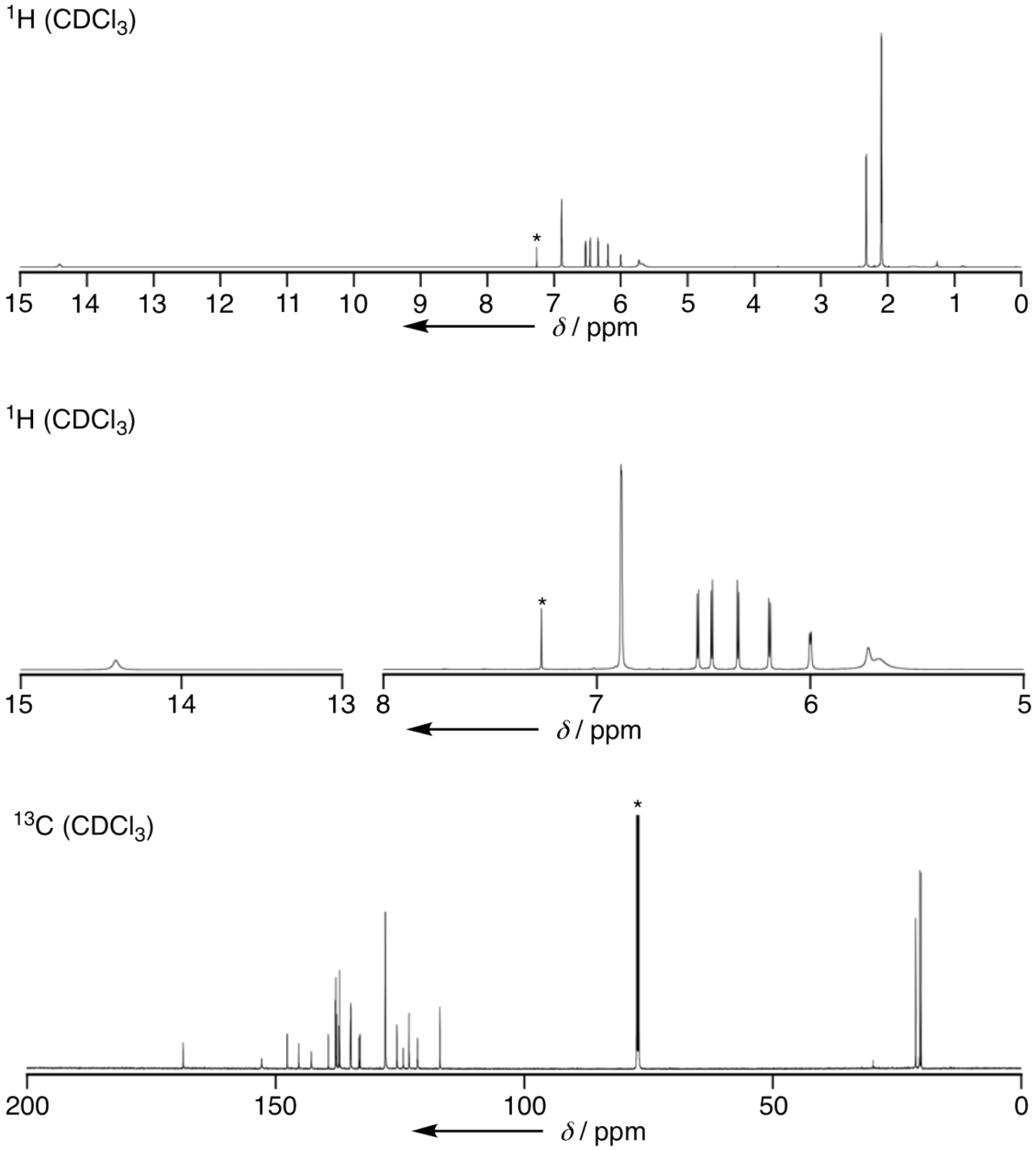

Figure S3-10-1. ^{1}H and ^{13}C NMR spectra of **9b** in and $CDCl_3$ at room temperature. * means residual solvent peaks.

A signal in ^{13}C NMR spectrum was not observed presumably because of their broadness or overlapping.

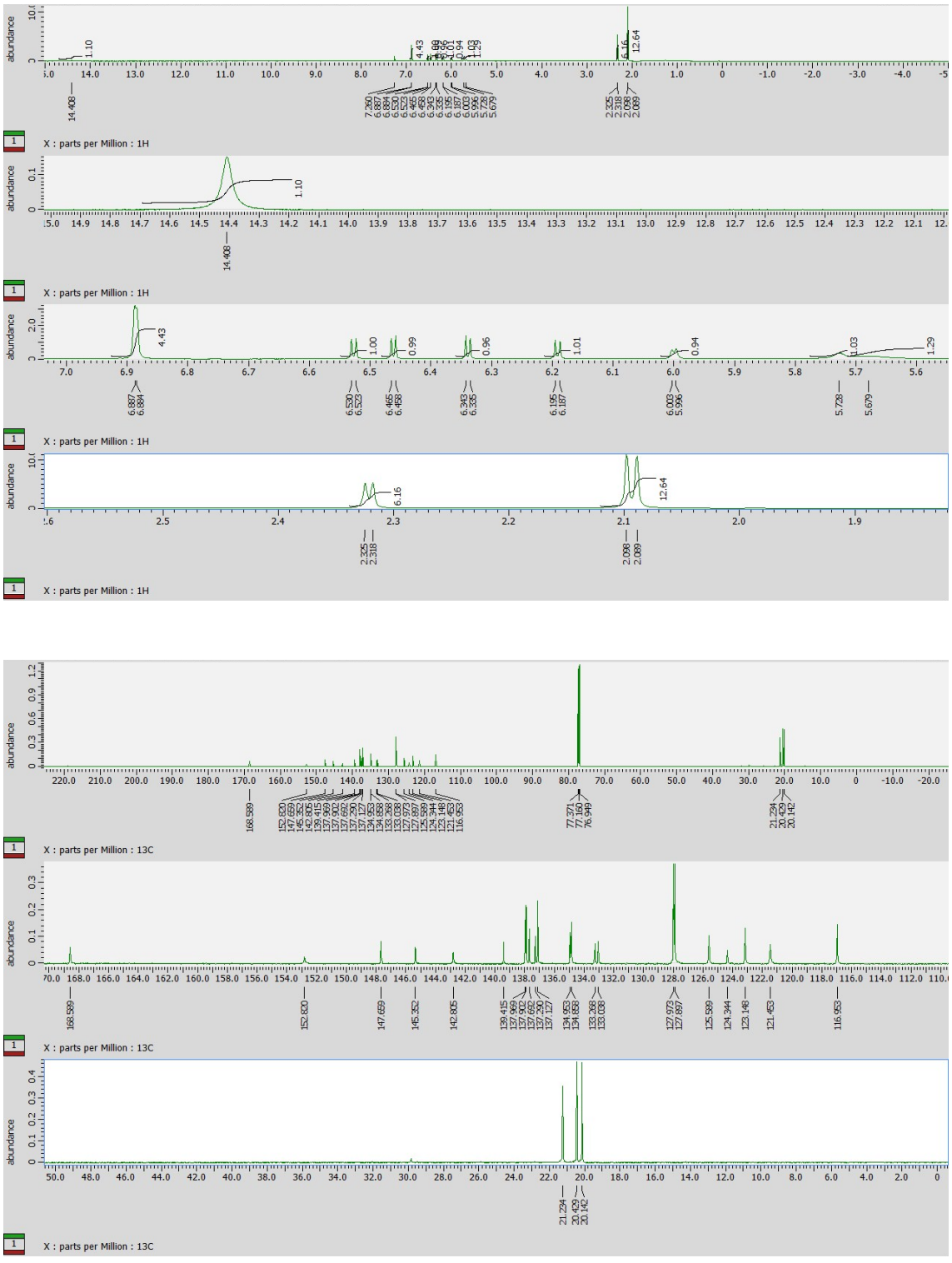

Figure S3-10-2. ^{1}H and ^{13}C NMR spectra of **9b** in and $CDCl_3$ at room temperature.

A signal in ^{13}C NMR spectrum was not observed presumably because of their broadness or overlapping.

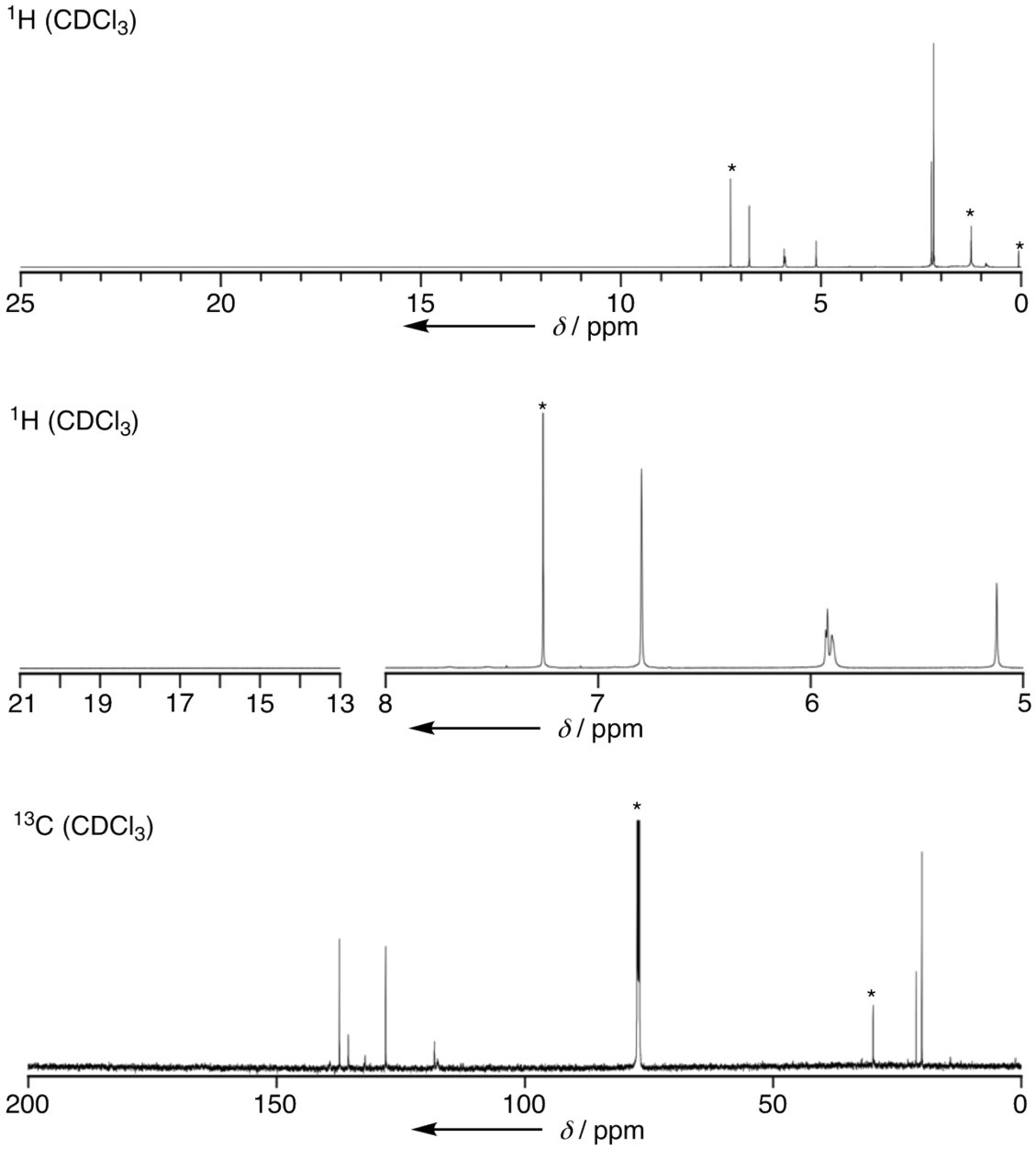

Figure S3-11-1. ^{1}H and ^{13}C NMR spectra of **10b** in $CDCl_3$ at room temperature. * means residual solvent peaks.

Some signals in ^{13}C NMR spectrum were not observed because of poor solubility.

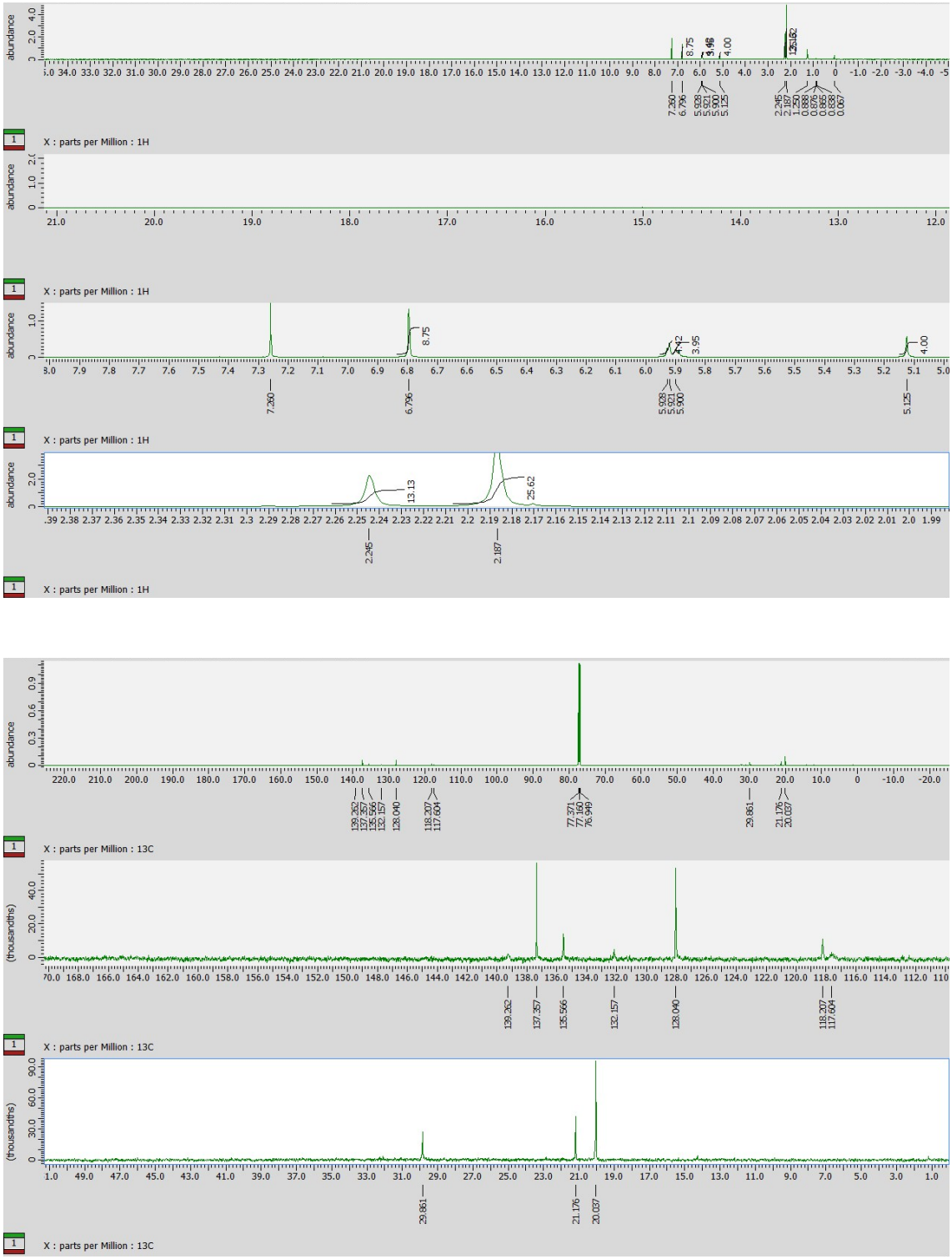

Figure S3-11-2. ^{1}H and ^{13}C NMR spectra of **10b** in $CDCl_3$ at room temperature.

Some signals in ^{13}C NMR spectrum were not observed because of poor solubility.

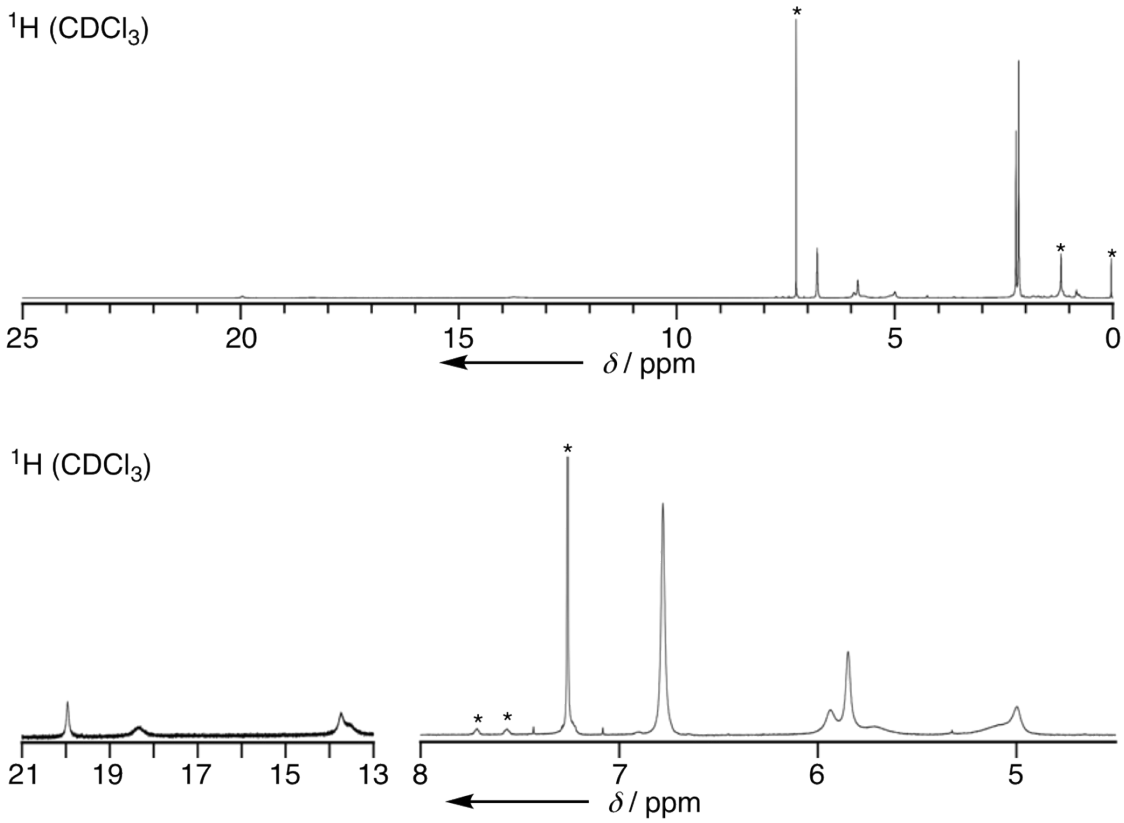

Figure S3-12-1. ^{1}H NMR spectra of **10b** in $CDCl_3$ at –60 ºC. * means residual solvent peaks.

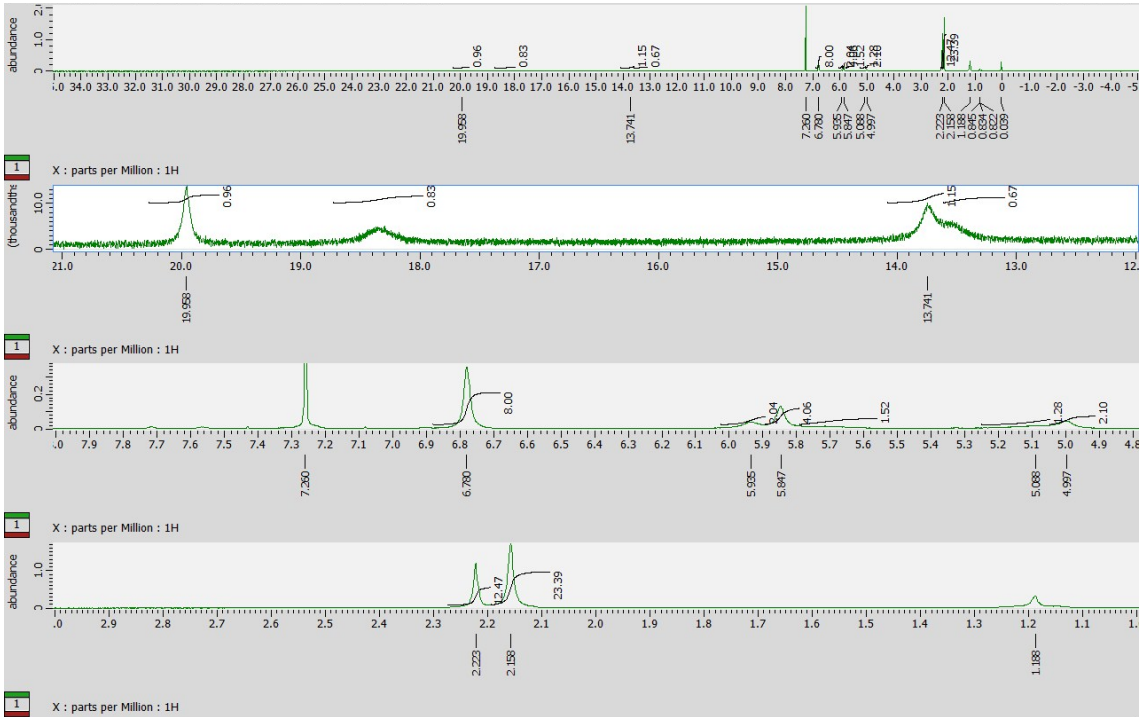

Figure S3-12-2. ^{1}H NMR spectra of **10b** in $CDCl_3$ at –60 ºC.

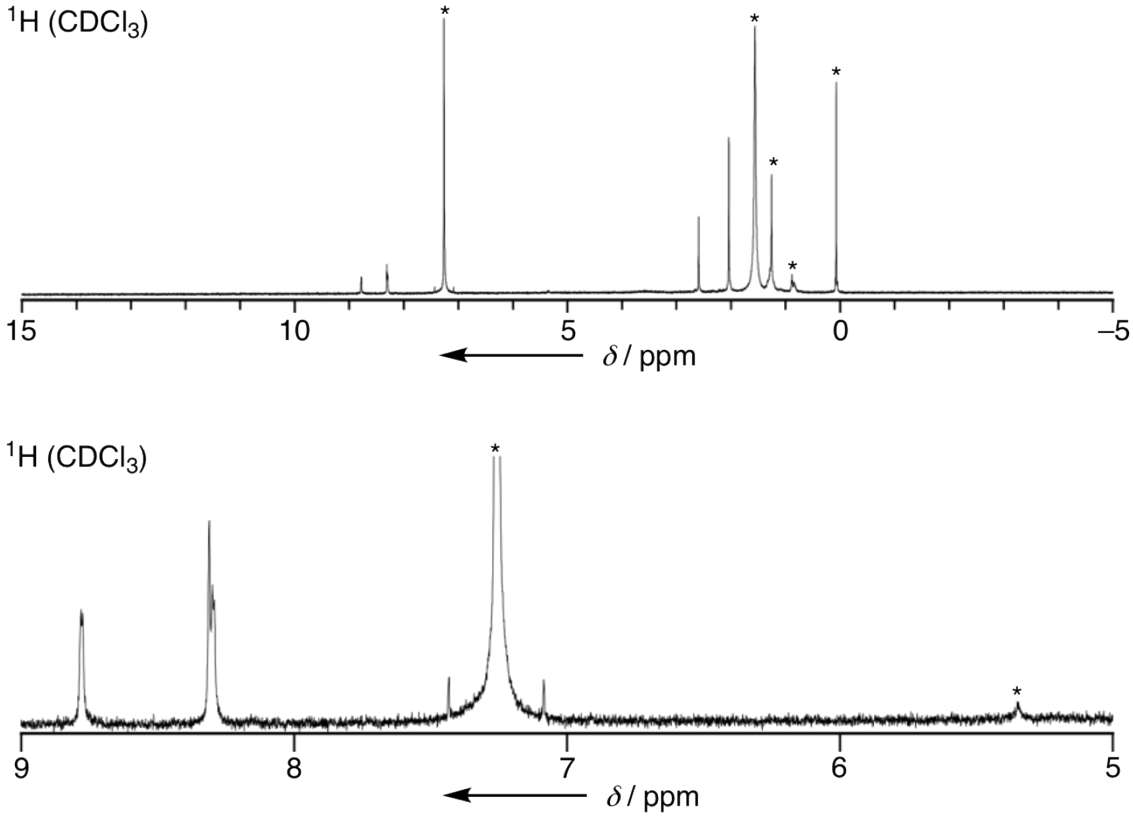

Figure S3-13-1. ^{1}H NMR spectra of **11b** in $CDCl_3$ at room temperature.

The signal assignable to NH protons was not observed presumably because of their broadness.

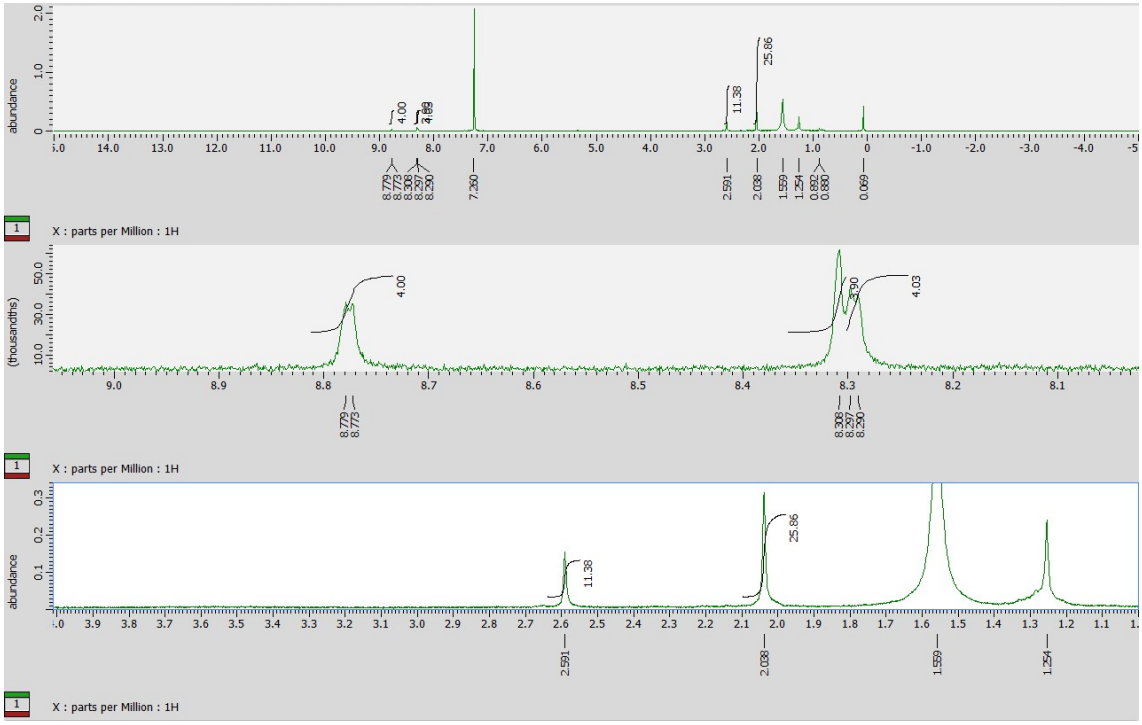

Figure S3-13-2. ^{1}H NMR spectra of **11b** in $CDCl_3$ at room temperature.

The signal assignable to NH protons was not observed presumably because of their broadness.

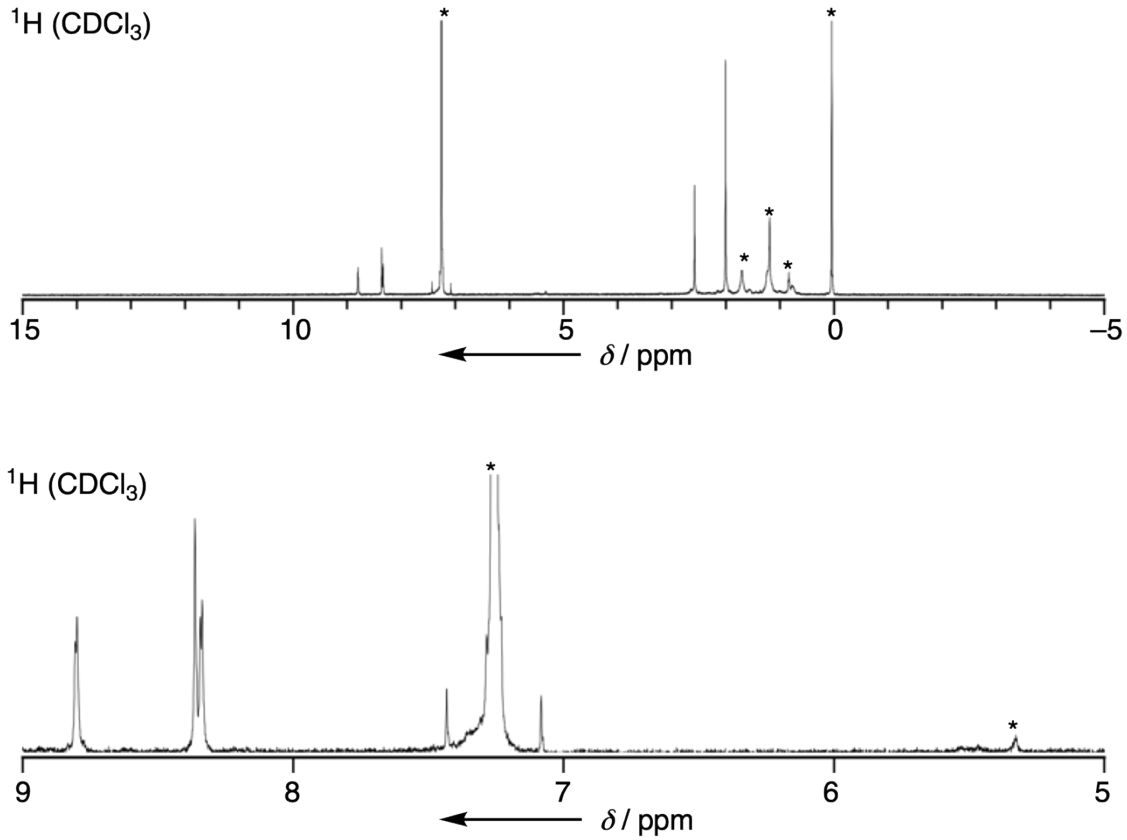

Figure S3-14-1. ^{1}H NMR spectra of **11b** in $CDCl_3$ at –60 ºC.

The signal assignable to NH protons was not observed presumably because of their broadness.

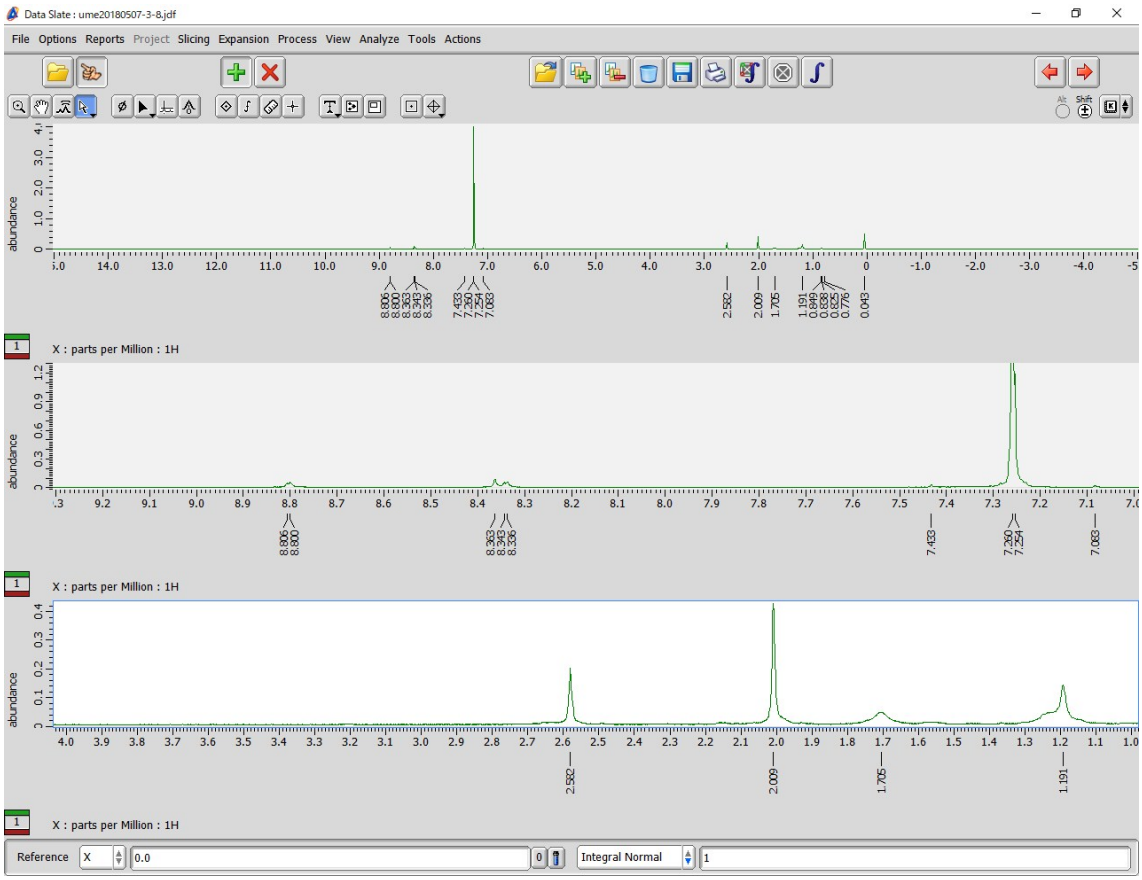

Figure S3-14-2. ^{1}H NMR spectra of **11b** in $CDCl_3$ at –60 ºC.

The signal assignable to NH protons was not observed presumably because of their broadness.

4. Mass Spectra

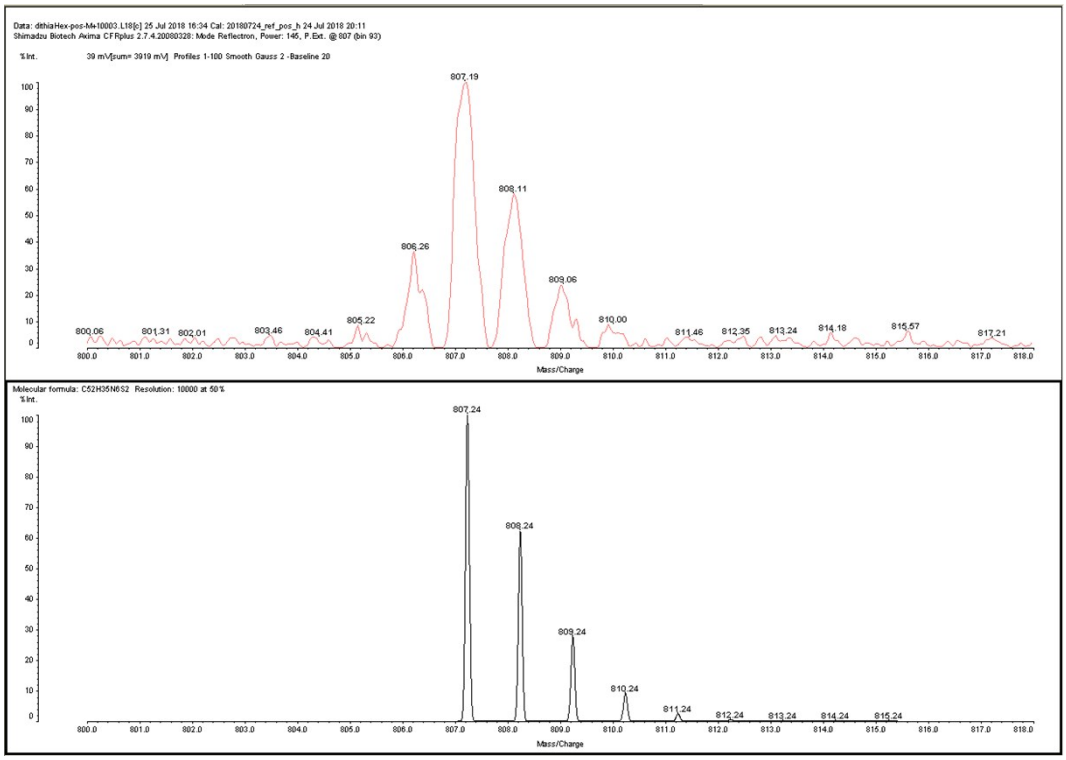

Figure S4-1. MALDI-TOF-MS of **8a**. (Top: observed; Bottom: simulated)

*The mass peaks were simulated as $[M+H]^+$ and a small contamination of $[M]$ appears at m/z = 806.26. Because of poor solubility, ESI-TOF-MS of **8a** was not obtained.

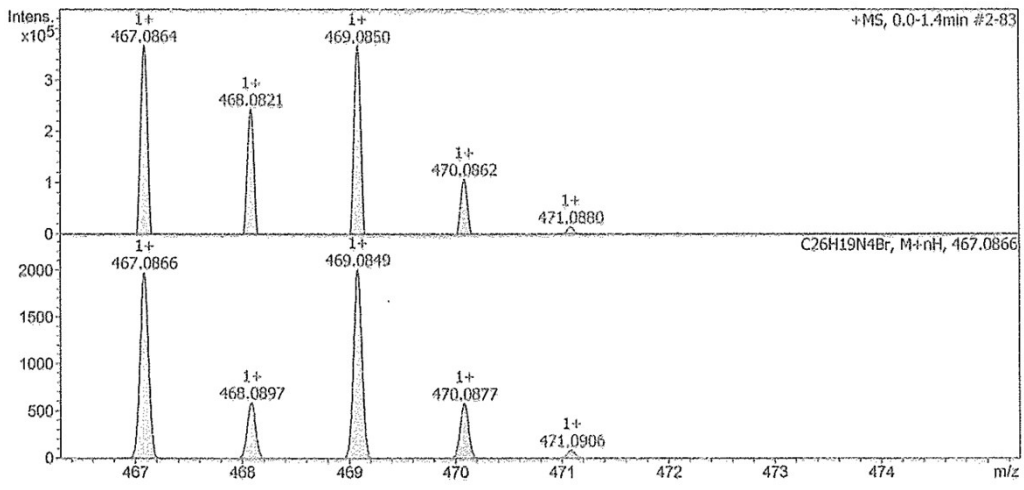

Figure S4-2. HR APCI-TOF-MS of **9a**. (Top: observed; Bottom: simulated)

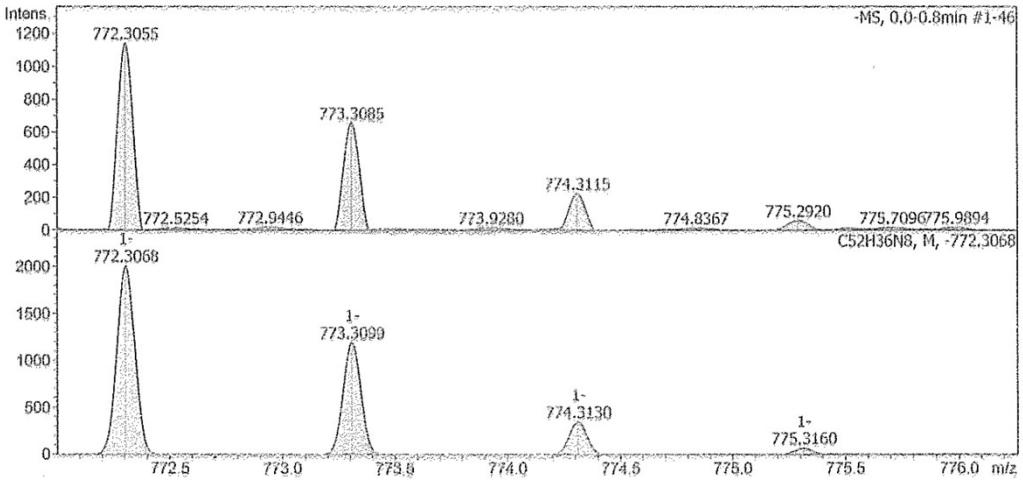

Figure S4-3. HR APCI-TOF-MS of **10a**. (Top: observed; Bottom: simulated)

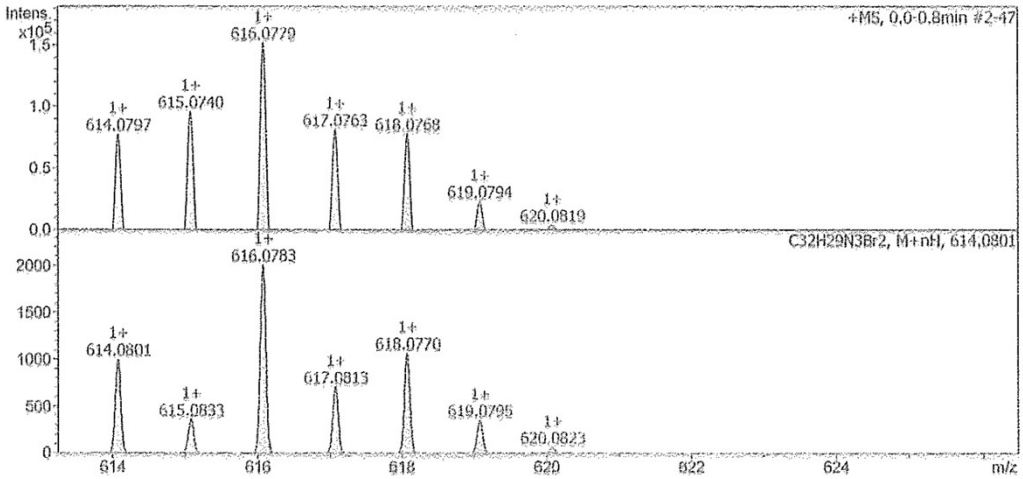

Figure S4-4. HR APCI-TOF-MS of **7b**. (Top: observed; Bottom: simulated)

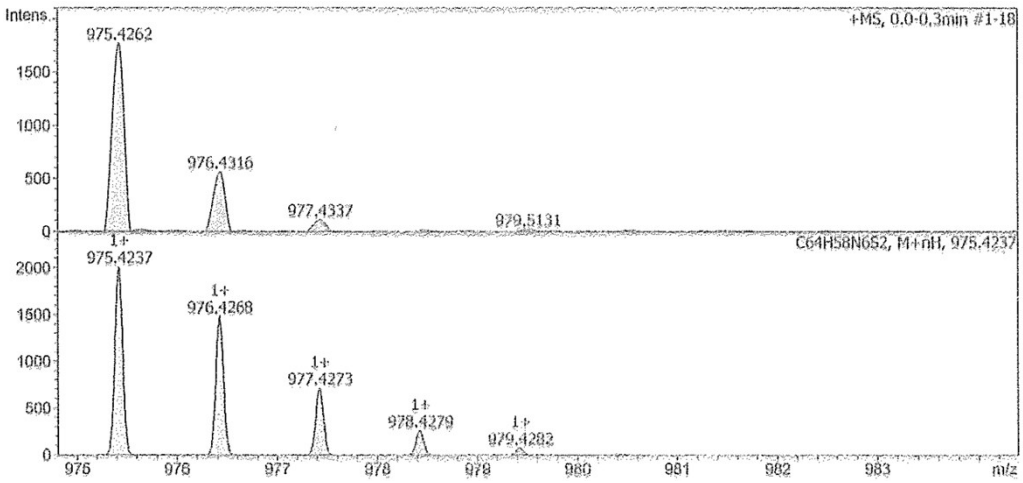

Figure S4-5. HR APCI-TOF-MS of **8b**. (Top: observed; Bottom: simulated)

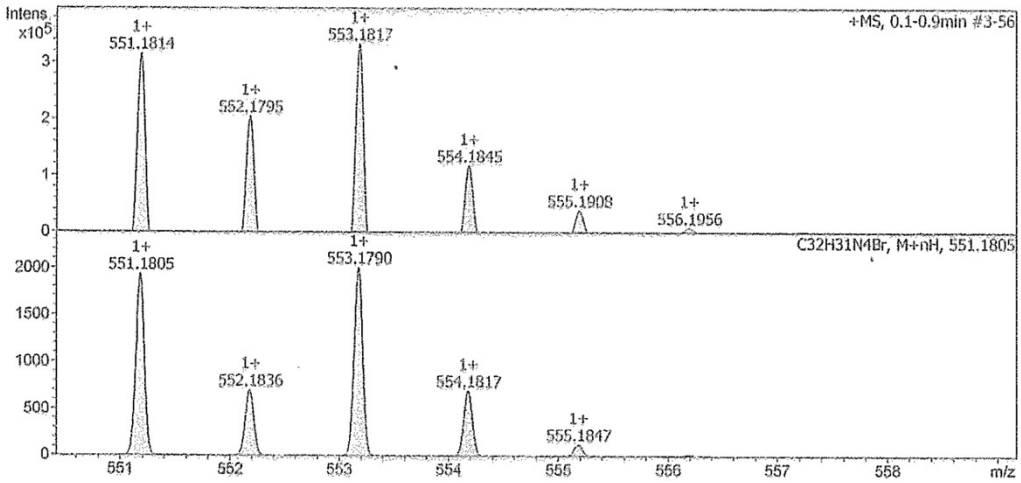

Figure S4-6. HR APCI-TOF-MS of **9b**. (Top: observed; Bottom: simulated)

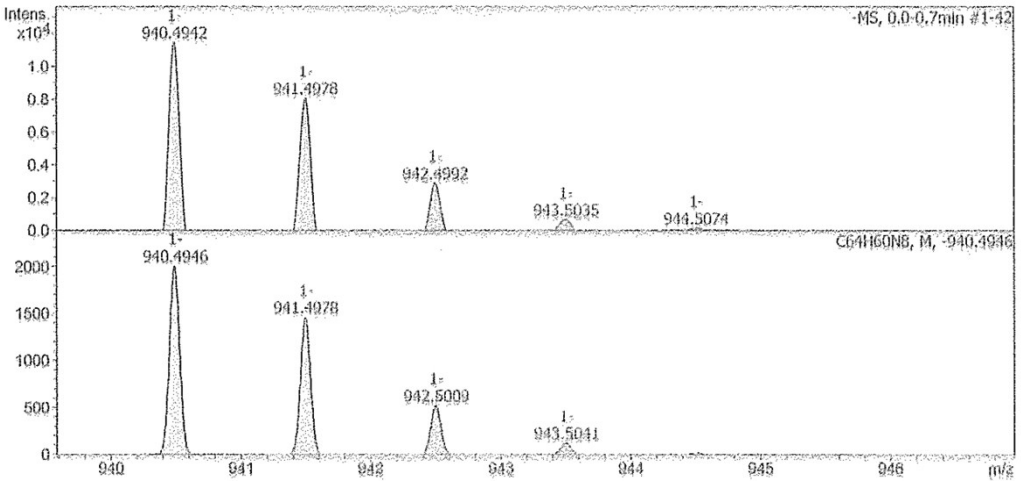

Figure S4-7. HR APCI-TOF-MS of **10b**. (Top: observed; Bottom: simulated)

5. X-Ray Crystallographic Details

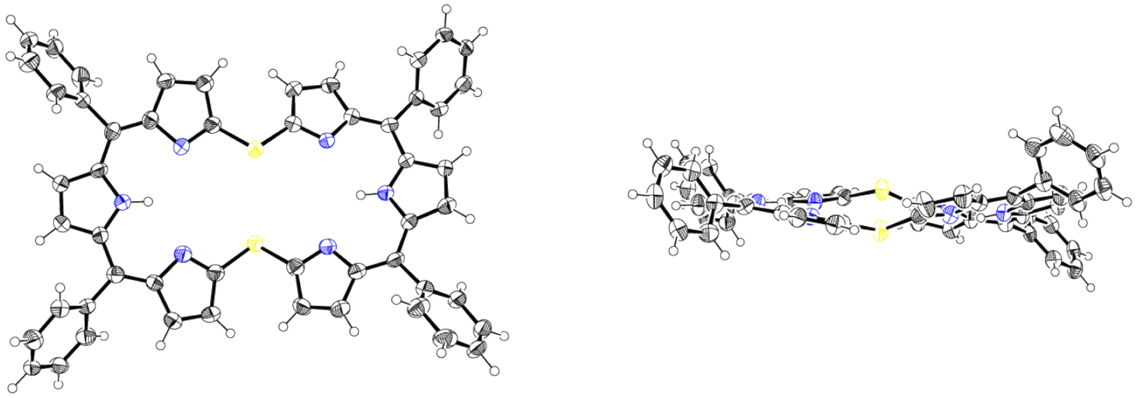

Figure S5-1. X-Ray crystal structure of **8a**. Thermal ellipsoids were scaled to 50% probability.

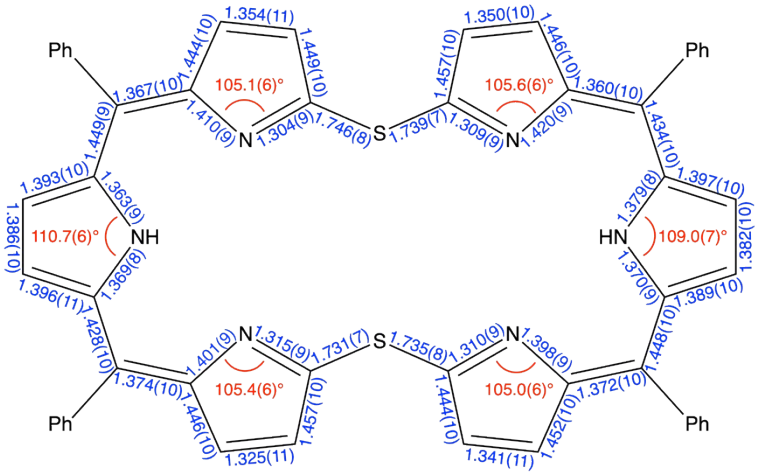

Figure S5-2. Bond lengths(Å) and bond angles of **8a**.

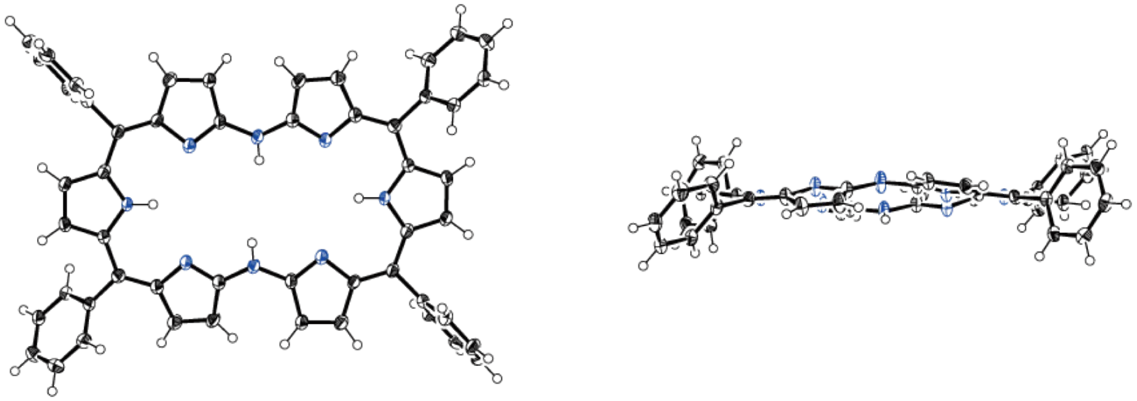

Figure S5-3. X-Ray crystal structure of **10a**. Solvent molecules were omitted for clarity. Thermal ellipsoids were scaled to 50% probability.

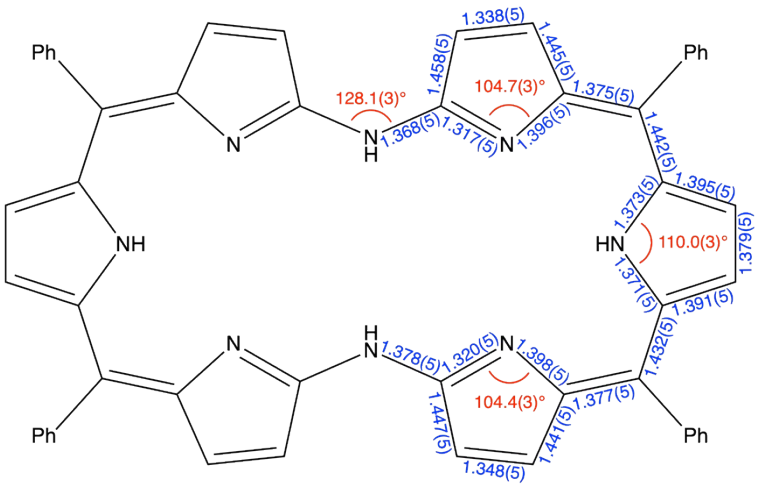

Figure S5-4. Bond lengths(Å) and bond angles of **10a**.

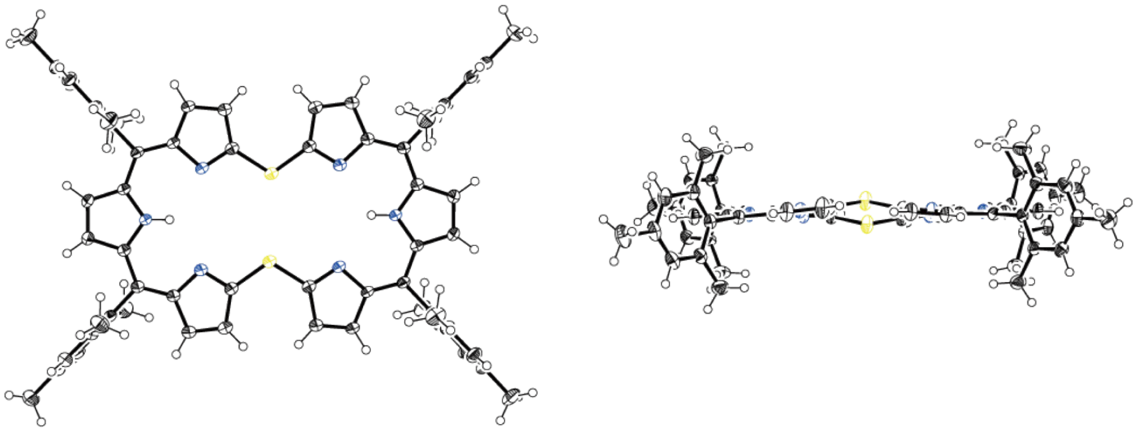

Figure S5-5. X-Ray crystal structure of **8b**. Solvent molecules were omitted for clarity. Thermal ellipsoids were scaled to 50% probability.

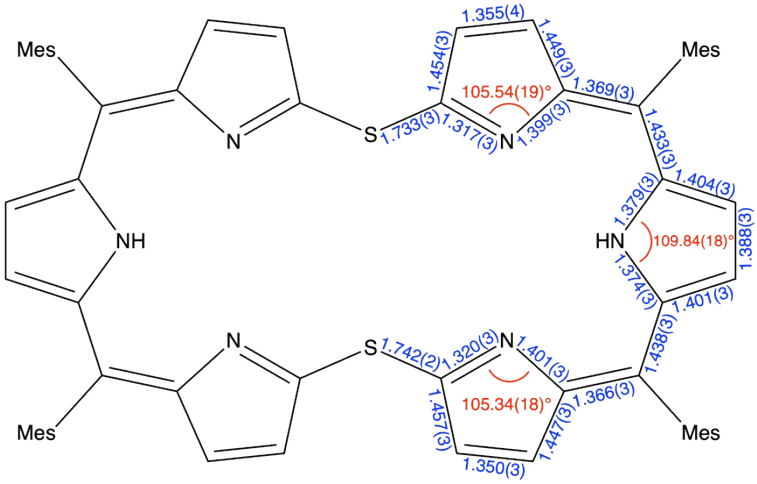

Figure S5-6. Bond lengths(Å) and bond angles of **8b**.

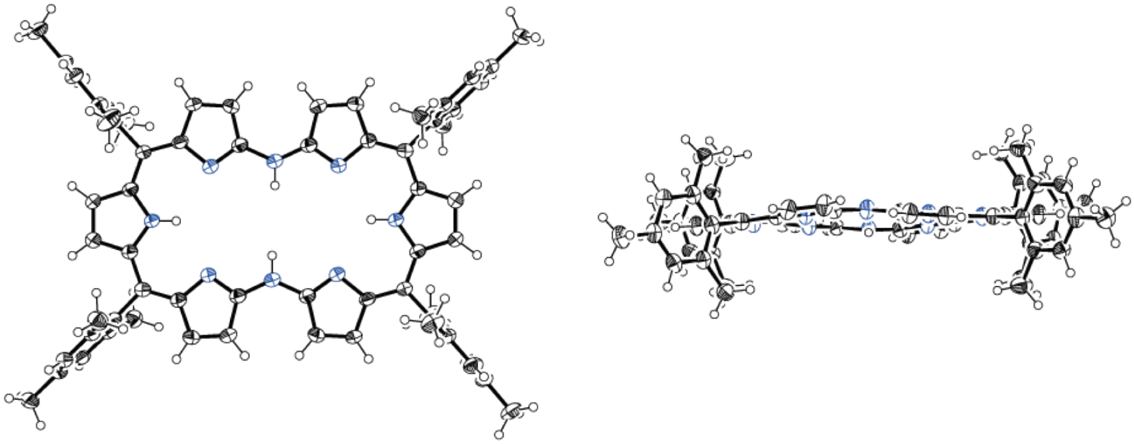

Figure S5-7. X-Ray crystal structure of **10b**. Solvent molecules were omitted for clarity. Thermal ellipsoids were scaled to 50% probability.

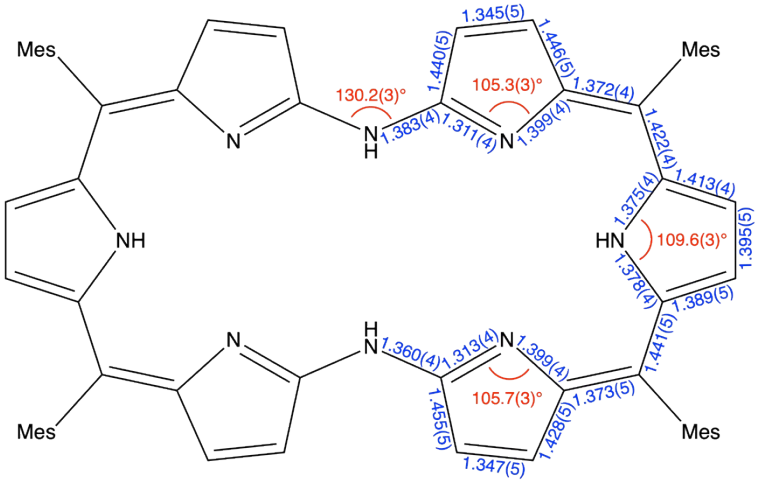

Figure S5-8. Bond lengths(Å) and bond angles of **10b**.

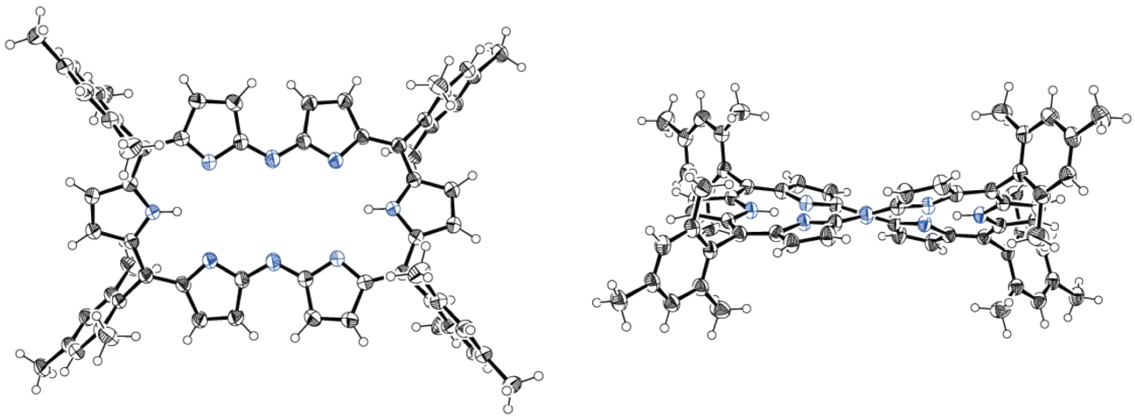

Figure S5-9. X-Ray crystal structure of **11b**. Hydrogen atoms except for NHs and solvent molecules were omitted for clarity. Thermal ellipsoids were scaled to 50% probability.

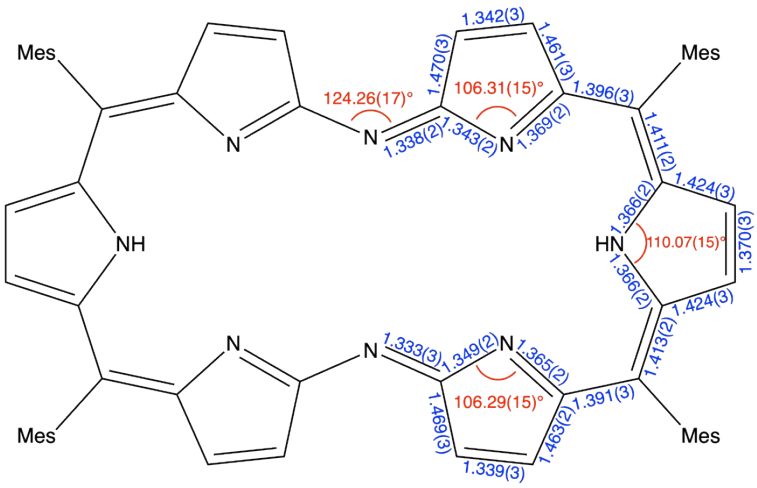

Figure S5-10. Bond lengths(Å) and bond angles of **11b**.

Note: All the hydrogen atoms are set via HFIX instructions with SHELXL-2014 program. In general, C–N–C bond angles of amine-type pyrrole and imine-type pyrrole are known to be around 110º and 105º, respectively. We assigned the positions of NHs by considering the C–N–C bond angles. It is important to note that the solid-state structure is not always the most stable form due to the presence of packing forces, or in some cases other isomer is stabilized by solvents in the solution state. The exact structural description for **10a,b** is still arguable. See also Figure S8-16.

Table S5-1. Crystal data and structure refinements for **8a** and **10a**.

Compound	**8a**	**10a**
Formula	$C_{52}H_{34}N_6S_2$	$C_{52}H_{36}N_8$, 0.696($CHCl_3$), 0.304($C_2H_4Cl_2$)
M_W	806.97	807.43
Crystal System	Orthorhombic	Monoclinic
Space Group	*P b c a* (No.61)	*P* $2_1/c$ (No.14)
a [Å]	17.555(7)	9.818(2)
b [Å]	19.539(7)	8.0037(16)
c [Å]	22.727(9)	28.018(6)
α [deg]	90	90
β [deg]	90	92.757(4)
γ [deg]	90	90
Volume [Å^3]	7796(5)	2199.1(8)
Z	8	2
Density [Mg/m^3]	1.375	1.338
Completeness	0.989	0.996
Goodness-of-fit	1.095	1.054
R_1 [$I > 2\sigma(I)$]	0.0642	0.0698
wR_2 (all data)	0.3486	0.2180
Solvent System	$CHCl_3$/MeOH	$CHCl_3$/MeOH
CCDC	1923183	1923184

Table S5-2. Crystal data and structure refinements for **8b**, **10b**, and **11b**.

Compound	**8b**	**10b**	**11b**
Formula	$C_{32}H_{29}N_3$, $CHCl_3$	$C_{32}H_{30}N_4$, 0.397(CH_2Cl_2), 0.603($CHCl_3$)	$C_{32}H_{29}N_4$, CH_2Cl_2
M_W	607.05	576.43	554.52
Crystal System	Monoclinic	Monoclinic	Monoclinic
Space Group	$P\,2_1/n$ (No.14)	$P\,2_1/n$ (No.14)	$P\,2/c$ (No.13)
a [Å]	13.8418(3)	13.6032(2)	13.2366(3)
b [Å]	16.1286(2)	15.9814(2)	13.5740(3)
c [Å]	14.8743(3)	14.9395(3)	16.9125(5)
α [deg]	90	90	90
β [deg]	115.395(2)	116.214(2)	108.153(3)
γ [deg]	90	90	90
Volume [Å^3]	2999.80(11)	2913.78(9)	2887.49(13)
Z	4	4	4
Density [Mg/m^3]	1.344	1.314	1.276
Completeness	0.984	0.995	0.959
Goodness-of-fit	1.097	1.038	1.041
R_1 [$I > 2\sigma(I)$]	0.0550	0.0887	0.0521
wR_2 (all data)	0.1607	0.3374	0.1609
Solvent System	$CHCl_3$/MeOH	CH_2Cl_2/$CHCl_3$ /MeOH	CH_2Cl_2/pyridine /*n*-heptane
CCDC	1923185	1923186	1923187

6. UV/Vis/NIR Absorption Spectra

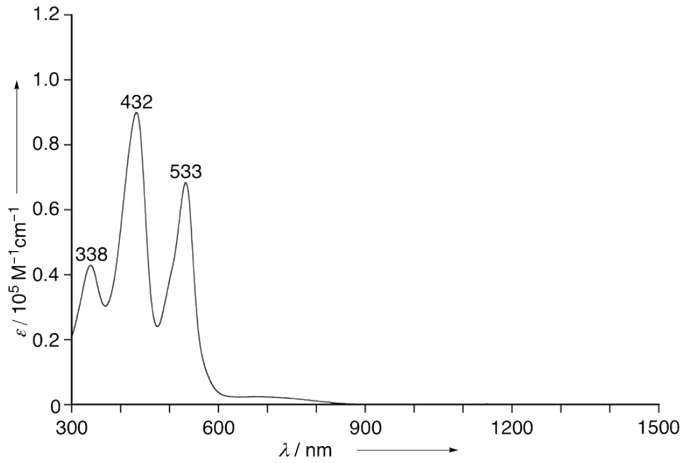

Figure S6-1. UV/Vis/NIR absorption spectrum of **8a** in CH_2Cl_2.

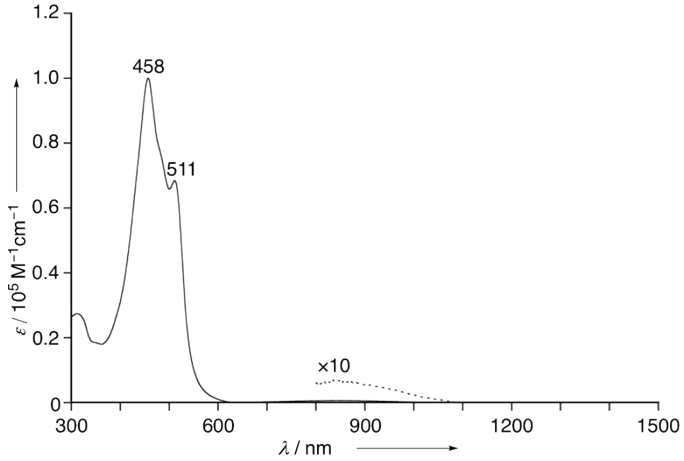

Figure S6-2. UV/Vis/NIR absorption spectrum of **10a** in CH_2Cl_2.

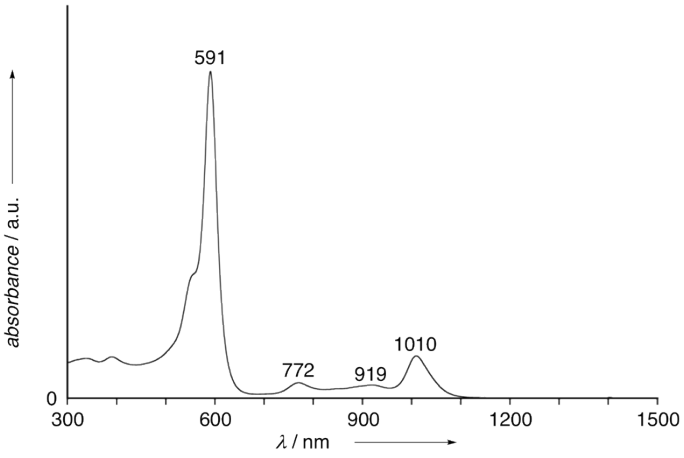

Figure S6-3. UV/Vis/NIR absorption spectrum of **11a** in CH_2Cl_2/pyridine.

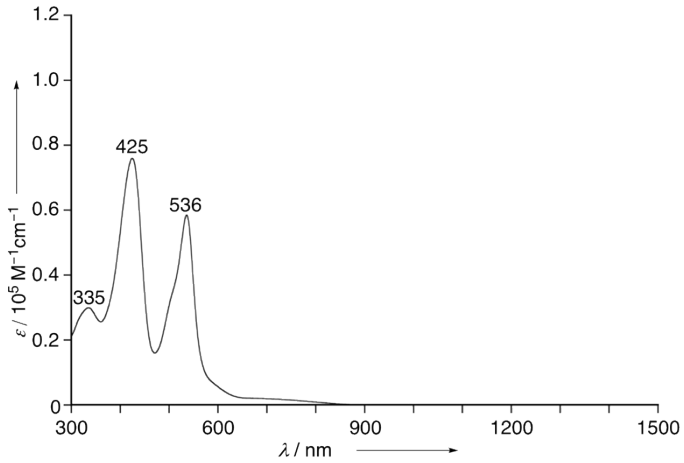

Figure S6-4. UV/Vis/NIR absorption spectrum of **8b** in CH_2Cl_2.

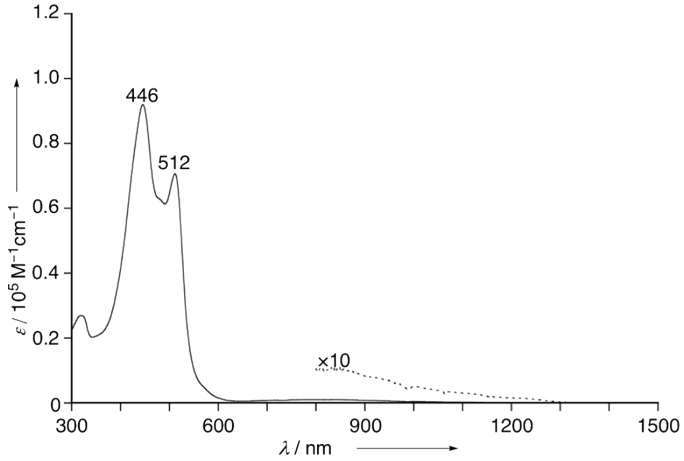

Figure S6-5. UV/Vis/NIR absorption spectrum of **10b** in CH_2Cl_2.

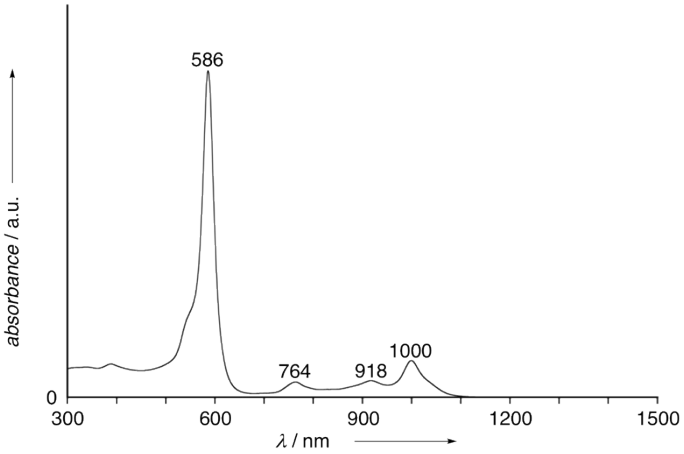

Figure S6-6. UV/Vis/NIR absorption spectrum of **11b** in CH_2Cl_2/pyridine.

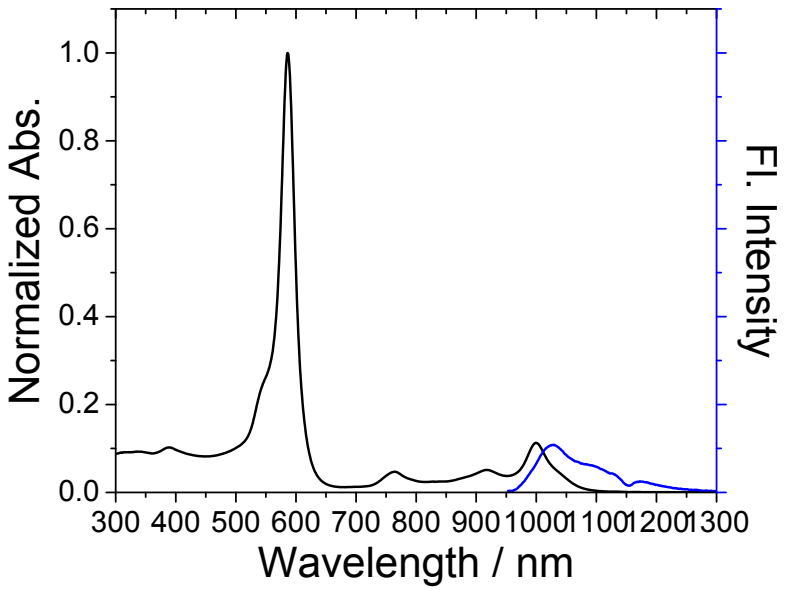

Figure S6-7. UV/Vis/NIR absorption and fluorescence spectra of **11b** in CH_2Cl_2/pyridine.

7. Cyclic Voltammograms

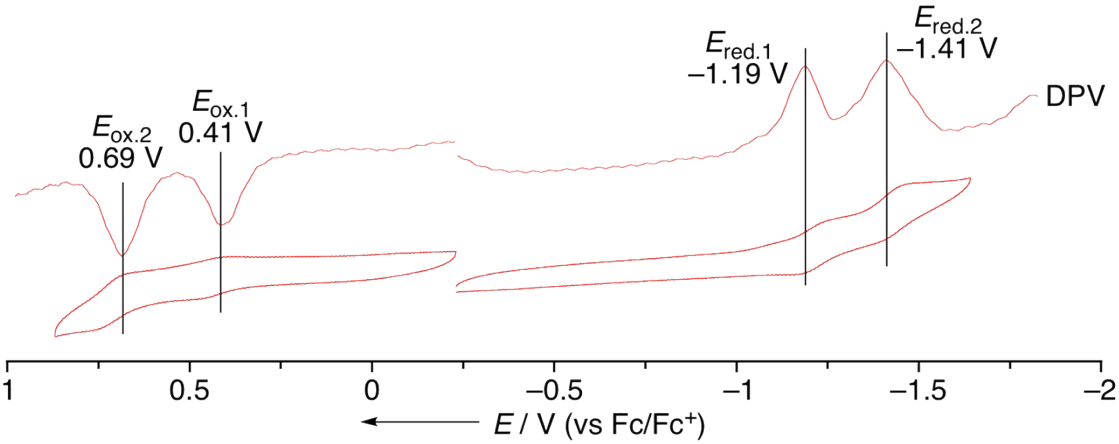

Figure S7-1. Cyclic voltammogram of **8a** measured in CH_2Cl_2.

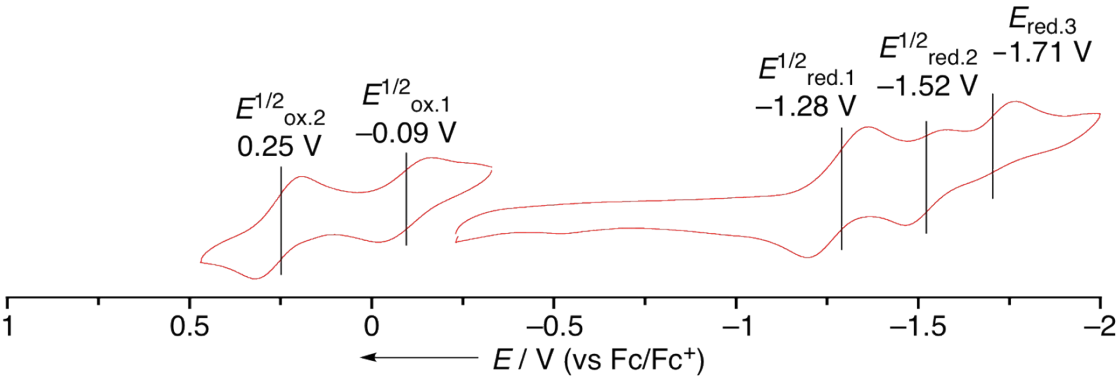

Figure S7-2. Cyclic voltammogram of **10a** measured in CH_2Cl_2.

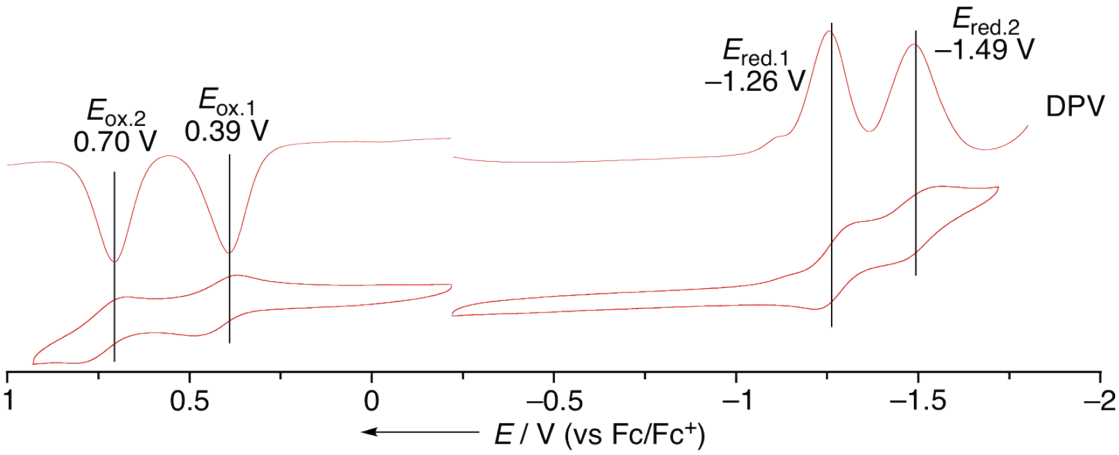

Figure S7-3. Cyclic voltammogram of **8b** measured in CH_2Cl_2.

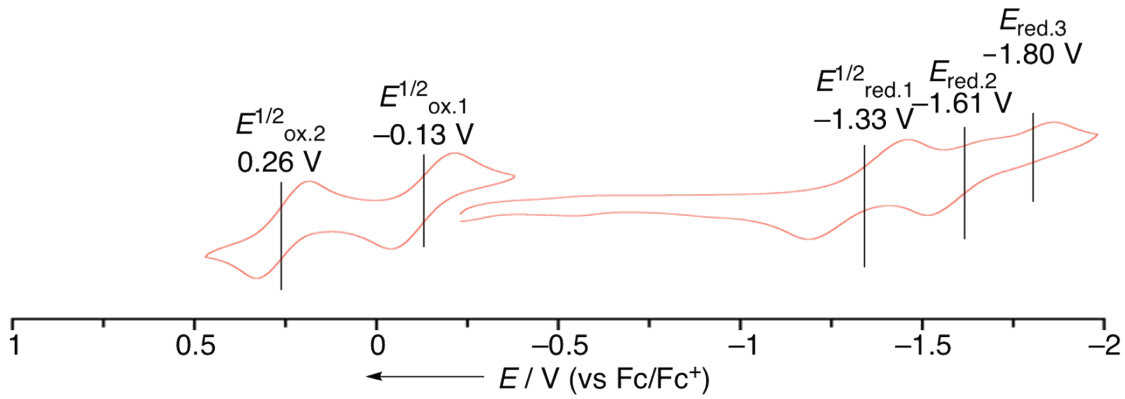

Figure S7-4. Cyclic voltammogram of **10b** measured in CH_2Cl_2.

Table S7. Summary of the redox potentials.

	$E^{1/2}_{ox.2}$ /V	$E^{1/2}_{ox.1}$ /V	$E^{1/2}_{red.1}$ /V	$E^{1/2}_{red.2}$ /V	$E^{1/2}_{red.3}$ /V	$E^{1/2}_{ox.1} - E^{1/2}_{red.1}$ /eV
8a	0.69	0.41	–1.19	–1.41	–	1.60
10a	0.25	–0.09	–1.28	–1.52	–1.71	1.19
8b	0.70	0.39	–1.26	–1.49	–	1.65
10b	0.26	–0.13	–1.33	–1.61	–1.80	1.20

Potentials[V] vs ferrocene/ferrocenium ion. Scan rate 0.05 Vs^{-1}; working electrode, glassy carbon; counter electrode, Pt wire; supporting electrolyte, 0.1 M $^{n}Bu_4NPF_6$; reference electrode, $Ag/AgNO_3$

8. DFT Calculations

All calculations were carried out using the *Gaussian 16* program.[S2] Initial geometries were obtained from X-ray structures. Calculations were performed by the density functional theory (DFT) method with restricted B3LYP (Becke's three-parameter hybrid exchange functionals and the Lee-Yang-Parr correlation functional)[S3] level, employing a basis sets 6-31G(d). NICS values were calculated with GIAO method at the B3LYP level employing a basis sets 6-31G(d).

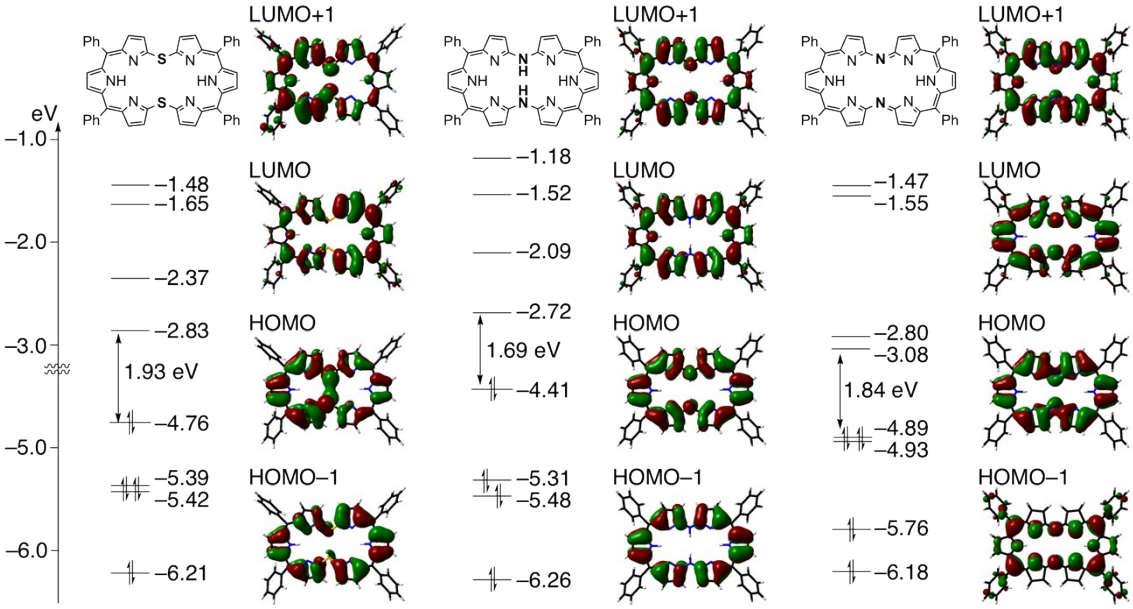

Figure S8-1. Kohn-Sham MO representations and energy diagrams of **8a**, **10a**, and **11a**.

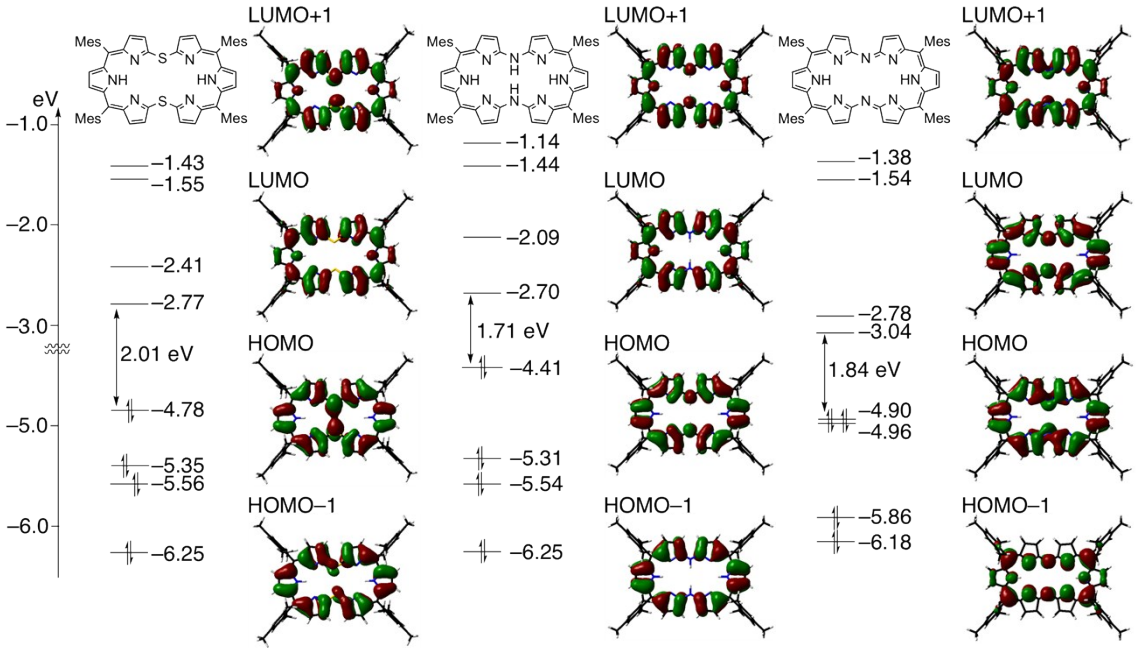

Figure S8-2. Kohn-Sham MO representations and energy diagrams of **8b**, **10b**, and **11b**.

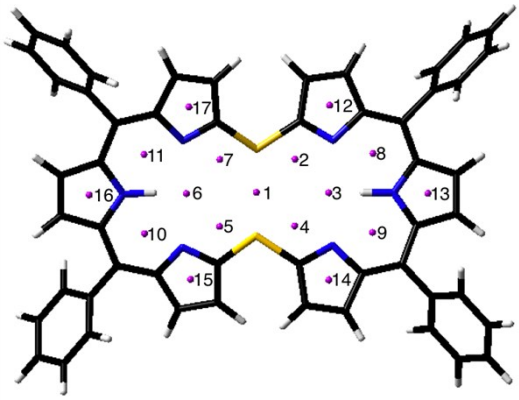

Position	NICS (ppm)	Position	NICS (ppm)	Position	NICS (ppm)	Position	NICS (ppm)
1	1.30	6	1.05	11	4.33	16	–8.70
2	1.60	7	–0.78	12	–3.03	17	–3.57
3	2.55	8	5.25	13	–8.07		
4	1.32	9	5.35	14	–2.65		
5	–1.32	10	3.76	15	–3.14		

Figure S8-3. NICS(0) values at various positions of **8a**.

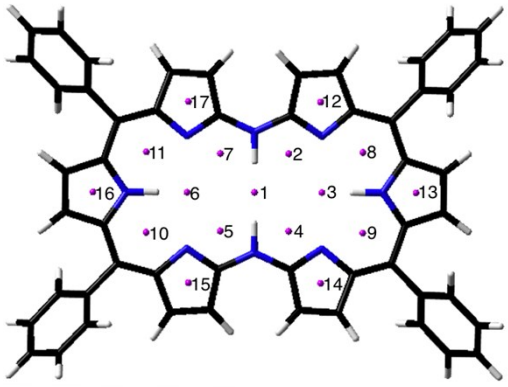

Position	NICS (ppm)	Position	NICS (ppm)	Position	NICS (ppm)	Position	NICS (ppm)
1	7.79	6	8.09	11	11.67	16	–5.94
2	7.78	7	7.81	12	–4.47	17	–4.56
3	8.09	8	11.56	13	–5.94		
4	7.81	9	11.67	14	–4.56		
5	7.78	10	11.56	15	–4.47		

Figure S8-4. NICS(0) values at various positions of **10a**.

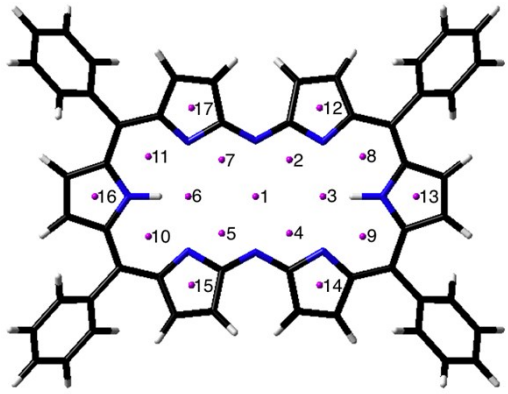

Position	NICS (ppm)	Position	NICS (ppm)	Position	NICS (ppm)	Position	NICS (ppm)
1	–12.34	6	–13.33	11	–15.11	16	–10.60
2	–12.38	7	–12.38	12	3.44	17	3.44
3	–13.33	8	–15.11	13	–10.60		
4	–12.38	9	–15.11	14	3.44		
5	–12.38	10	–15.11	15	3.44		

Figure S8-5. NICS(0) values at various positions of **11a**.

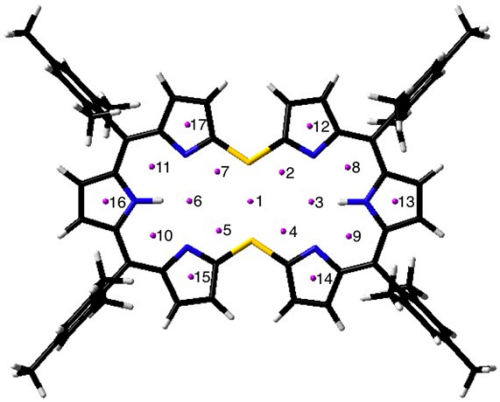

Position	NICS (ppm)	Position	NICS (ppm)	Position	NICS (ppm)	Position	NICS (ppm)
1	2.10	6	2.11	11	5.33	16	–8.21
2	0.61	7	0.97	12	–2.95	17	–3.41
3	2.11	8	4.98	13	–8.21		
4	0.97	9	5.33	14	–3.41		
5	0.61	10	4.98	15	–2.95		

Figure S8-6. NICS(0) values at various positions of **8b**.

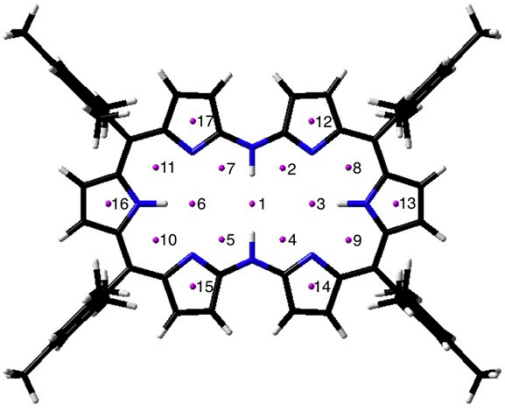

Position	NICS (ppm)	Position	NICS (ppm)	Position	NICS (ppm)	Position	NICS (ppm)
1	7.75	6	8.04	11	11.67	16	–6.02
2	7.75	7	7.75	12	–4.08	17	–4.08
3	8.04	8	11.67	13	–6.02		
4	7.75	9	11.67	14	–4.08		
5	7.75	10	11.67	15	–4.08		

Figure S8-7. NICS(0) values at various positions of **10b**.

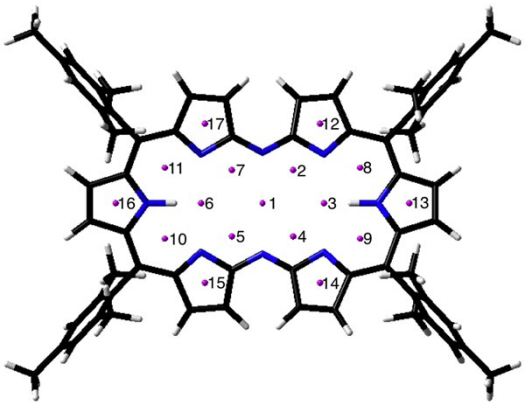

Position	NICS (ppm)	Position	NICS (ppm)	Position	NICS (ppm)	Position	NICS (ppm)
1	–12.40	6	–13.44	11	–15.17	16	–10.54
2	–12.61	7	–12.61	12	4.31	17	4.31
3	–13.44	8	–15.17	13	–10.54		
4	–12.61	9	–15.17	14	4.31		
5	–12.61	10	–15.17	15	4.31		

Figure S8-8. NICS(0) values at various positions of **11b**.

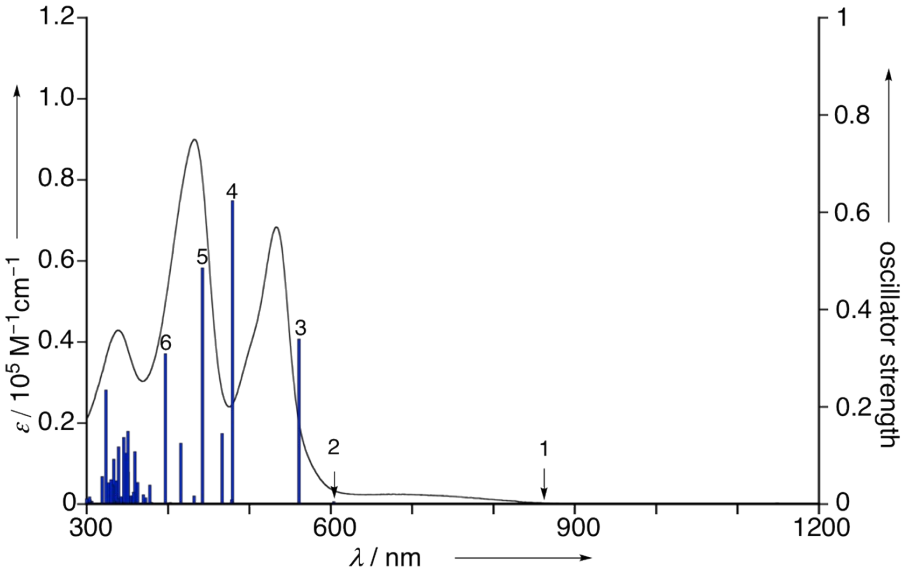

Figure S8-9. Calculated absorption spectrum on the basis of optimized structure (bar) and observed absorption spectra (line) of **8a**.

Table S8-1. Selected excitation energies of **8a** calculated at B3LYP/6-31G(d) level.

No	Wavelength (nm)	Coefficients	Electronic transition	*f*
1	864.23	0.70400	210(HOMO) -> 211(LUMO)	0.0019
2	603.48	0.42490	209(HOMO–1) -> 211(LUMO)	0.0058
		0.55455	210(HOMO) -> 212(LUMO+1)	
3	560.75	0.66624	208(HOMO–2) -> 211(LUMO)	0.3404
		0.15631	209(HOMO–1) -> 211(LUMO)	
		0.14474	210(HOMO) -> 213(LUMO+2)	
4	478.91	–0.12136	208(HOMO–2) -> 211(LUMO)	0.6248
		0.50862	209(HOMO–1) -> 211(LUMO)	
		0.25867	209(HOMO–1) -> 212(LUMO+1)	
		–0.39916	210(HOMO) -> 212(LUMO+1)	
5	442.13	–0.10232	203(HOMO–7) -> 211(LUMO)	0.4864
		–0.11727	208(HOMO–2) -> 211(LUMO)	
		0.65572	210(HOMO) -> 213(LUMO+2)	
		0.15462	210(HOMO) -> 214(LUMO+2)	
6	396.60	0.29618	203(HOMO–7) -> 211(LUMO)	0.3101
		0.52748	206(HOMO–4) -> 211(LUMO)	
		0.12683	208(HOMO–2) -> 212(LUMO+1)	
		–0.24526	210(HOMO) -> 214(LUMO+3)	

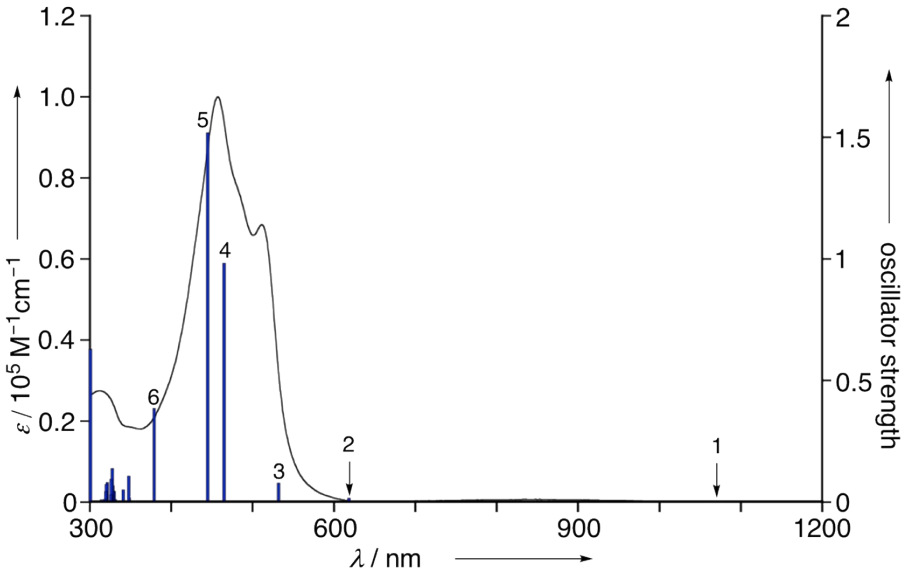

Figure S8-10. Calculated absorption spectrum on the basis of optimized structure (bar) and observed absorption spectra (line) of **10a**.

Table S8-2. Selected excitation energies of **10a** calculated at B3LYP/6-31G(d) level.

No	Wavelength (nm)	Coefficients	Electronic transition	*f*
1	1072.03	0.70679	202(HOMO) -> 203(LUMO)	0.0000
2	617.99	0.39724	201(HOMO–1) -> 203(LUMO)	0.0179
		0.58363	202(HOMO) -> 204(LUMO+1)	
3	531.77	0.58784	200(HOMO–2) -> 203(LUMO)	0.0797
		–0.38069	202(HOMO) -> 205(LUMO+2)	
4	464.58	0.58683	201(HOMO–1) -> 203(LUMO)	0.9842
		–0.40579	202(HOMO) -> 204(LUMO+1)	
		0.10653	202(HOMO) <- 204(LUMO+1)	
5	444.40	0.12362	197(HOMO–5) -> 203(LUMO)	1.5197
		0.35836	200(HOMO–2) -> 203(LUMO)	
		0.57991	202(HOMO) -> 205(LUMO+2)	
6	378.73	0.67701	197(HOMO–5) -> 203(LUMO)	0.3865
		–0.10862	200(HOMO–2) -> 203(LUMO)	

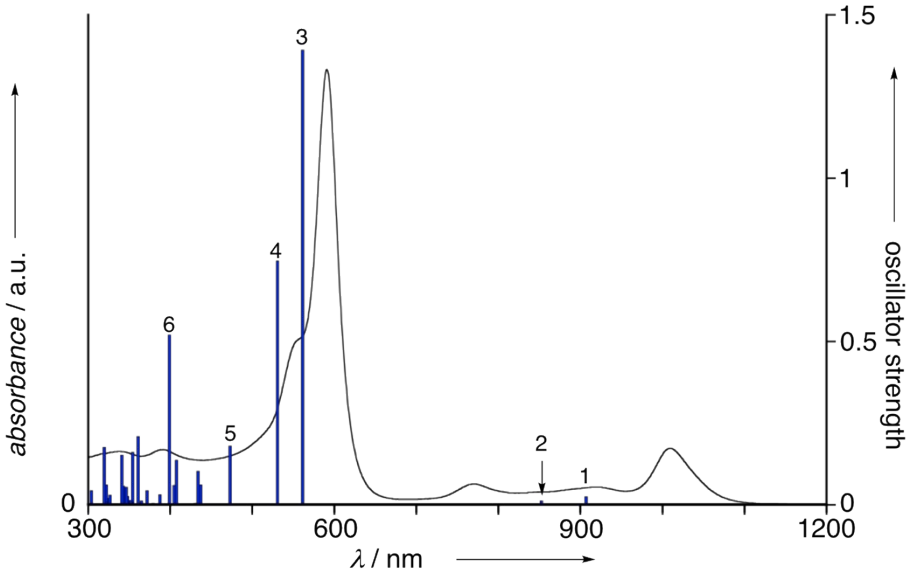

Figure S8-11. Calculated absorption spectrum on the basis of optimized structure (bar) and observed absorption spectra (line) of **11a**.

Table S8-3. Selected excitation energies of **11a** calculated at B3LYP/6-31G(d) level.

No	Wavelength (nm)	Coefficients	Electronic transition	*f*
1	906.71	–0.42961	200(HOMO–1) -> 203(LUMO+1)	0.0256
		0.55936	201(HOMO) -> 202(LUMO)	
2	852.32	0.55921	200(HOMO–1) -> 202(LUMO)	0.0136
		0.43168	201(HOMO) -> 203(LUMO+1)	
3	561.33	–0.17101	193(HOMO–8) -> 202(LUMO)	1.3937
		0.12537	197(HOMO–4) -> 202(LUMO)	
		0.53554	200(HOMO–1) -> 203(LUMO+1)	
		0.40293	201(HOMO) -> 202(LUMO)	
		–0.10446	200(HOMO–1) <- 203(LUMO+1)	
		–0.13570	201(HOMO) <- 202(LUMO)	
4	530.54	0.13957	197(HOMO–4) -> 203(LUMO+1)	0.7476
		–0.43794	200(HOMO–1) -> 202(LUMO)	
		0.55428	201(HOMO) -> 203(LUMO+1)	
		0.14692	200(HOMO–1) <- 202(LUMO)	
		–0.13113	201(HOMO) <- 203(LUMO+1)	
5	472.92	0.67098	197(HOMO–4) -> 202(LUMO)	0.1809
		–0.11985	201(HOMO) -> 202(LUMO)	
6	398.67	0.13118	190(HOMO) -> 203(LUMO+1)	0.5210
		0.19837	191(HOMO) -> 202(LUMO)	
		0.25624	193(HOMO–8) -> 202(LUMO)	

	0.58029	196(HOMO–5) -> 203(LUMO+1)
	0.12326	200(HOMO–1) -> 203(LUMO+1)

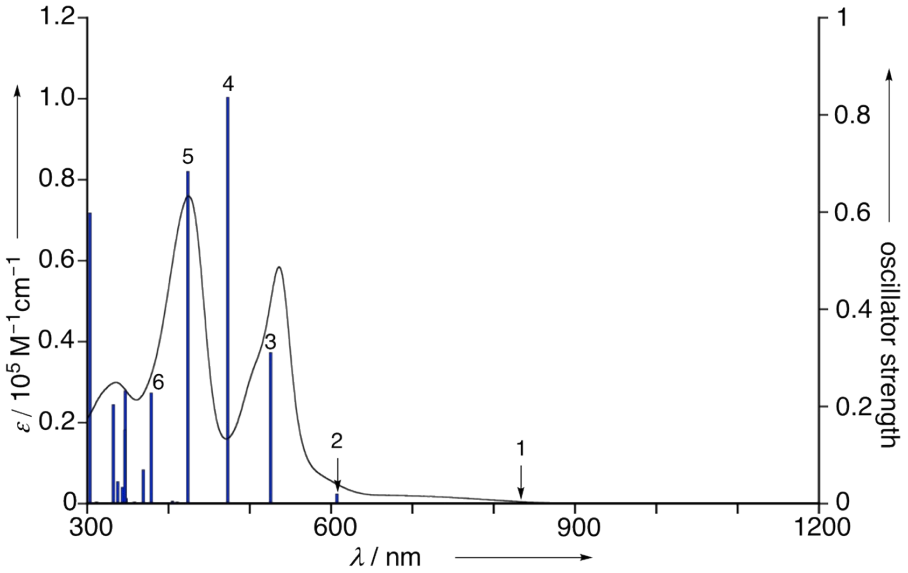

Figure S8-12. Calculated absorption spectrum on the basis of optimized structure (bar) and observed absorption spectra (line) of **8b**.

Table S8-3. Selected excitation energies of **8b** calculated at B3LYP/6-31G(d) level.

No	Wavelength (nm)	Coefficients	Electronic transition	*f*
1	833.20	0.70541	258(HOMO) -> 259(LUMO)	0.0000
2	606.85	0.40824	257(HOMO-1) -> 259(LUMO)	0.0211
		0.57365	258(HOMO) -> 260(LUMO+1)	
3	525.41	0.61553	256(HOMO–2) -> 259(LUMO)	0.3121
		0.25312	257(HOMO–1) -> 259(LUMO)	
		–0.12505	258(HOMO) -> 260(LUMO+1)	
		–0.17578	258(HOMO) -> 261(LUMO+2)	
4	472.56	–0.27703	256(HOMO–2) -> 259(LUMO)	0.8372
		0.52034	257(HOMO–1) -> 259(LUMO)	
		–0.39988	258(HOMO) -> 260(LUMO+1)	
		0.10023	258(HOMO) <- 260(LUMO+1)	
5	423.48	0.12765	244(HOMO–14) -> 259(LUMO)	0.6848
		0.14691	256(HOMO–2) -> 259(LUMO)	
		0.66191	258(HOMO) -> 261(LUMO+2)	
6	378.55	0.58046	244(HOMO–14) -> 259(LUMO)	0.2285
		0.23371	245(HOMO–13) -> 259(LUMO)	
		0.19499	246(HOMO–12) -> 260(LUMO+1)	
		–0.14060	255(HOMO–3) -> 260(LUMO+1)	
		–0.12804	257(HOMO–1) -> 262(LUMO+3)	

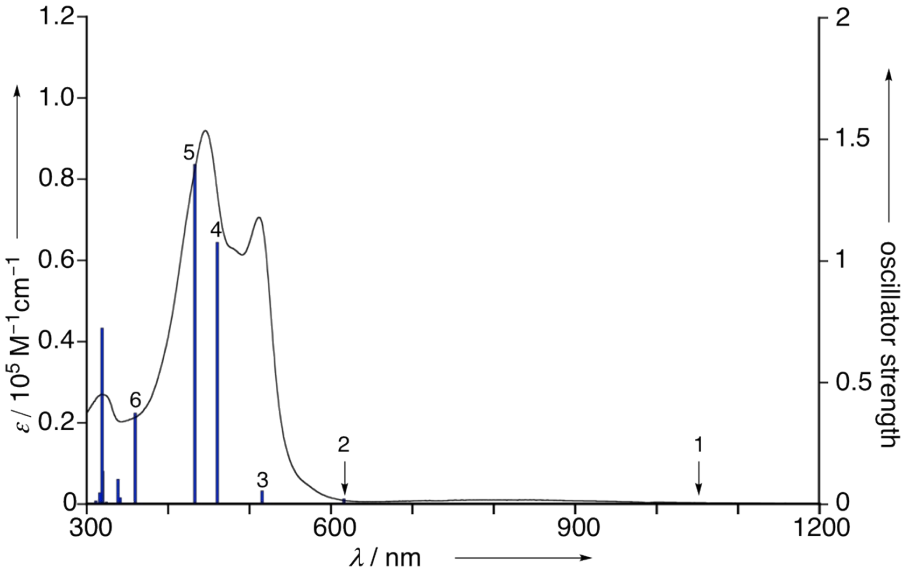

Figure S8-13. Calculated absorption spectrum on the basis of optimized structure (bar) and observed absorption spectra (line) of **10b**.

Table S8-4. Selected excitation energies of **10b** calculated at B3LYP/6-31G(d) level.

No	Wavelength (nm)	Coefficients	Electronic transition	*f*
1	1055.17	0.70686	250(HOMO) -> 251(LUMO)	0.0000
2	616.11	–0.39305	249(HOMO–1) -> 251(LUMO)	0.0237
		0.58698	250(HOMO) -> 252(LUMO+1)	
3	515.25	0.58490	248(HOMO–2) -> 251(LUMO)	0.0561
		0.38895	250(HOMO) -> 253(LUMO+2)	
4	460.20	0.59296	249(HOMO–1) -> 251(LUMO)	1.0783
		0.40262	250(HOMO) -> 252(LUMO+1)	
		–0.10871	250(HOMO) <- 252(LUMO+1)	
5	432.74	–0.13867	236(HOMO–14) -> 251(LUMO)	1.3988
		–0.36143	248(HOMO–2) -> 251(LUMO)	
		0.57313	250(HOMO) -> 253(LUMO+2)	
6	359.32	0.67368	236(HOMO–14) -> 251(LUMO)	0.3771
		–0.11093	248(HOMO–2) -> 251(LUMO)	
		–0.11913	249(HOMO–1) -> 254(LUMO+3)	

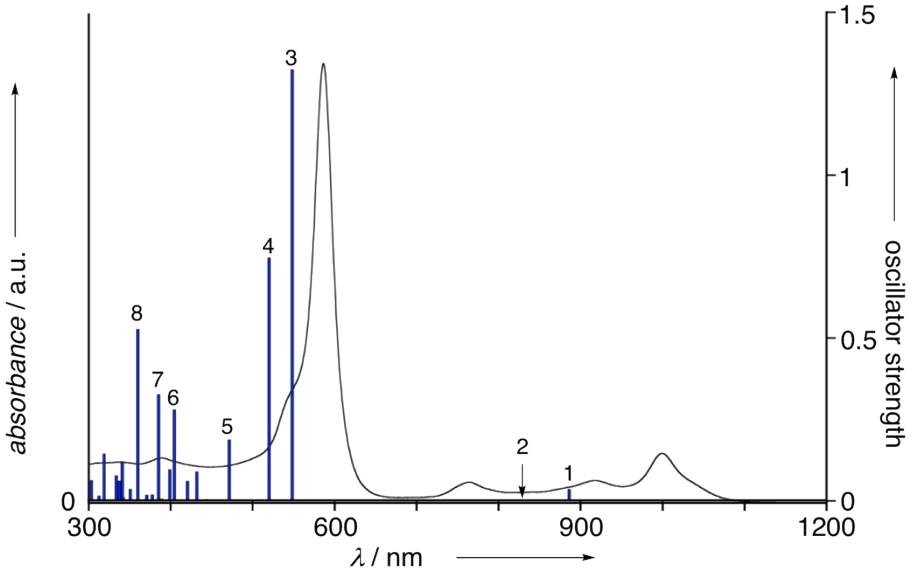

Figure S8-14. Calculated absorption spectrum on the basis of optimized structure (bar) and observed absorption spectra (line) of **11b**.

Table S8-5. Selected excitation energies of **11b** calculated at B3LYP/6-31G(d) level.

No	Wavelength (nm)	Coefficients	Electronic transition	*f*
1	886.01	0.42944	248(HOMO–1) -> 251(LUMO+1)	0.0358
		0.55983	249(HOMO) -> 250(LUMO)	
2	827.29	0.54814	248(HOMO–1) -> 250(LUMO)	0.0025
		–0.44538	249(HOMO) -> 251(LUMO+1)	
3	548.13	–0.20719	233(HOMO–16) -> 250(LUMO)	1.3252
		0.10138	236(HOMO–13) -> 251(LUMO+1)	
		–0.11682	245(HOMO–4) -> 250(LUMO)	
		0.53003	248(HOMO–1) -> 251(LUMO+1)	
		–0.39798	249(HOMO) -> 250(LUMO)	
		–0.10403	248(HOMO–1) <- 251(LUMO+1)	
		0.13300	249(HOMO) <- 250(LUMO)	
4	519.98	0.11278	236(HOMO–13) -> 250(LUMO)	0.7468
		0.15411	245(HOMO–4) -> 251(LUMO+1)	
		0.44735	248(HOMO–1) -> 250(LUMO)	
		0.53971	249(HOMO) -> 251(LUMO+1)	
		–0.14729	248(HOMO–1) <- 250(LUMO)	
		–0.13071	249(HOMO) <- 251(LUMO+1)	
5	471.27	0.11752	233(HOMO–16) -> 250(LUMO)	0.1881
		0.66684	245(HOMO–4) -> 250(LUMO)	
		–0.12399	249(HOMO) -> 250(LUMO)	

6	404.23	0.60940	233(HOMO–16) -> 250(LUMO)	0.2811
		0.19424	236(HOMO–13) -> 251(LUMO+1)	
		0.12820	244(HOMO–5) -> 251(LUMO+1)	
		–0.17530	245(HOMO–4) -> 250(LUMO)	
		0.10372	248(HOMO–1) -> 251(LUMO+1)	
		–0.10624	249(HOMO) -> 250(LUMO)	
7	385.19	0.12487	228(HOMO–21) -> 250(LUMO)	0.3277
		–0.27546	232(HOMO–17) -> 251(LUMO+1)	
		–0.19968	233(HOMO–16) -> 250(LUMO)	
		0.56328	236(HOMO–13) -> 251(LUMO+1)	
		0.11749	244(HOMO–5) -> 251(LUMO+1)	
		–0.10298	248(HOMO–1) -> 251(LUMO+1)	
8	359.55	0.57372	228(HOMO–21) -> 250(LUMO)	0.5274
		–0.27337	232(HOMO–17) -> 251(LUMO+1)	
		–0.22595	236(HOMO–13) -> 251(LUMO+1)	

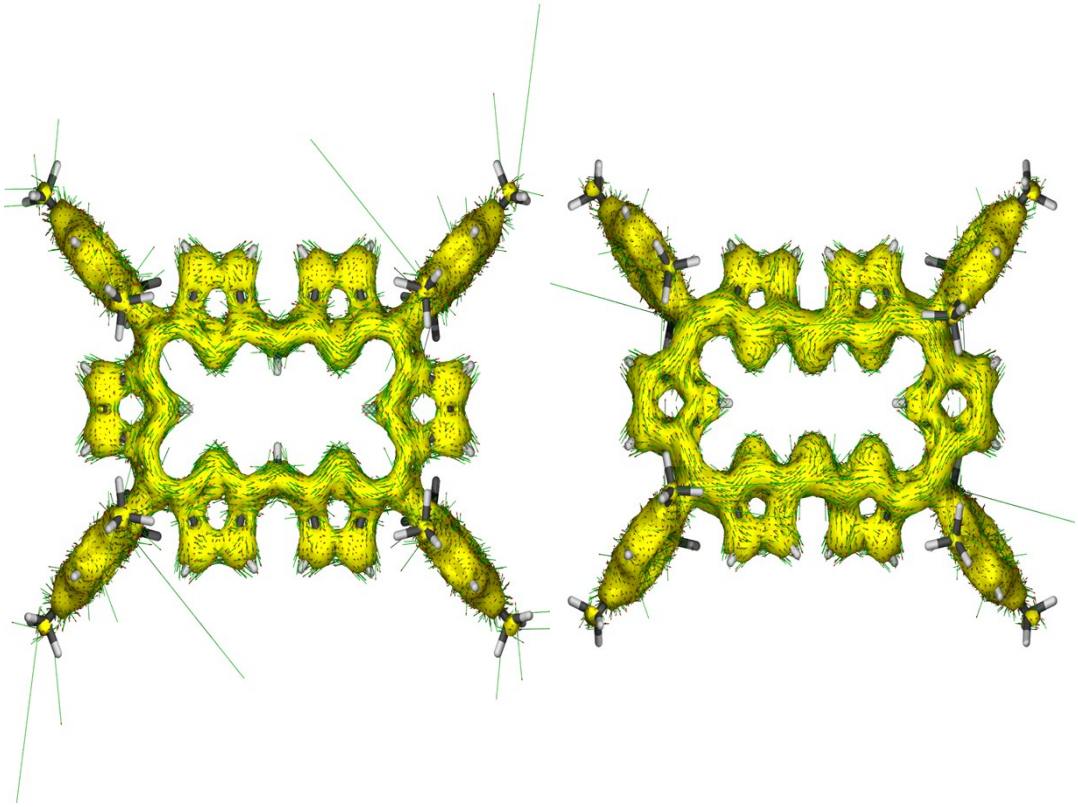

Figure S8-15. ACID plots for **10b** (left) and **11b** (right).[S4]

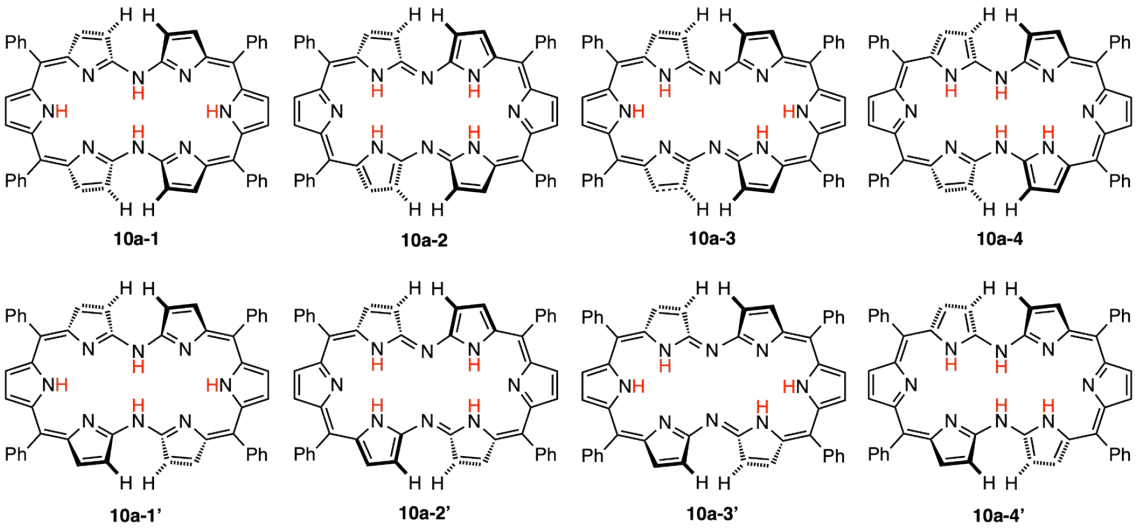

Figure S8-16. Calculated structures of isomers of **10a**.

Table S8-6. Total energy estimation including zero-point energy correction for isomers of **10a.**

structure	Total energy (hartree)	Relative energy (kcal/mol)
10a-1	–2440.439862	0
10a-2	–2440.442204	–1.47
10a-3	–2440.431938	+4.97
10a-4	–2440.409067	+19.32
10a-1'	–2440.442014	–1.35
10a-2'	–2440.449094	–5.79
10a-3'	–2440.434135	+3.59
10a-4'	–2440.409336	+19.16

***10a-1** was obtained from crystal structure.

*Accordingly, **10a-2'** was calculated to be the most stable form, but **10a-2** and **10a-2'** were also more stable than **10a-1** which was obtained from the crystal structure. At room temperature, isomerization among these isomers would be quite fast, eventually showing an averaged ^{1}H NMR spectra with C_s symmetry. At low temperature, although not clear, the structural isomerization, *e.g.* between **10a-2** and **10a-2'**, and/or NH tautomerization was restricted, leading to the symmetry reduction to C_2 symmetry as shown in Figure S3-4, S3-5 and S3-12.

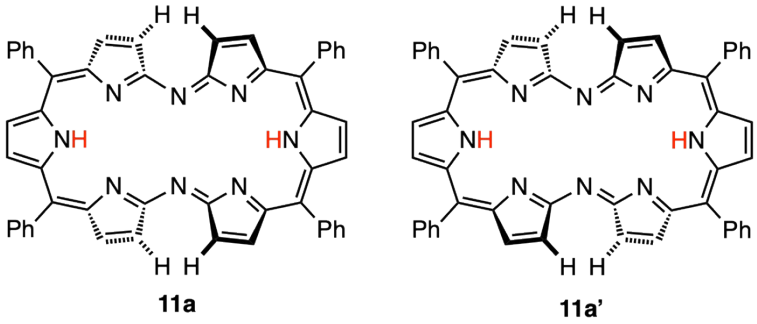

Figure S8-17. Calculated structures of isomers of **11a**.

Table S8-7. Total energy estimation including zero-point energy correction for isomers of **11a.**

structure	Total energy (hartree)	Relative energy (kcal/mol)
11a	–2439.198714	0
11a'	–2439.202995	–2.69

*The structure of **11a'** was constructed on the basis of the crystal structure of **11b'**.

9. Femtosecond Transient Absorption Spectra and Decay Profiles

The femtosecond transient absorption spectra were measured with pump-probe spectrometer, whichis consisted of Optical Parametric Amplifiers (Palitra, Quantronix) pumped by a Ti:sapphire regenerative amplifier system (Integra-C, Quantronix) operating at 1 kHz repetition rate and an optical detection system. The generated OPA pulses had a pulse width of ~ 100 fs and an average power of 100 mW in the range 280-2700 nm which were used as pump pulses. White light continuum (WLC) probe pulses were generated using a sapphire window (3 mm of thickness) by focusing of small portion of the fundamental 800 nm pulses which was picked off by a quartz plate before entering to the OPA.[S5]

After the measurements, we carefully checked absorption spectra of all compounds to detect if there were artifacts due to degradation and photo-oxidation of samples. HPLC grade solvents were used in all measurements. The three-dimensional data sets of ΔA versus time and wavelength were subjected to singular value decomposition and global fitting to obtain the kinetic time constants and their associated spectra using Surface Xplorer software (Ultrafast Systems).

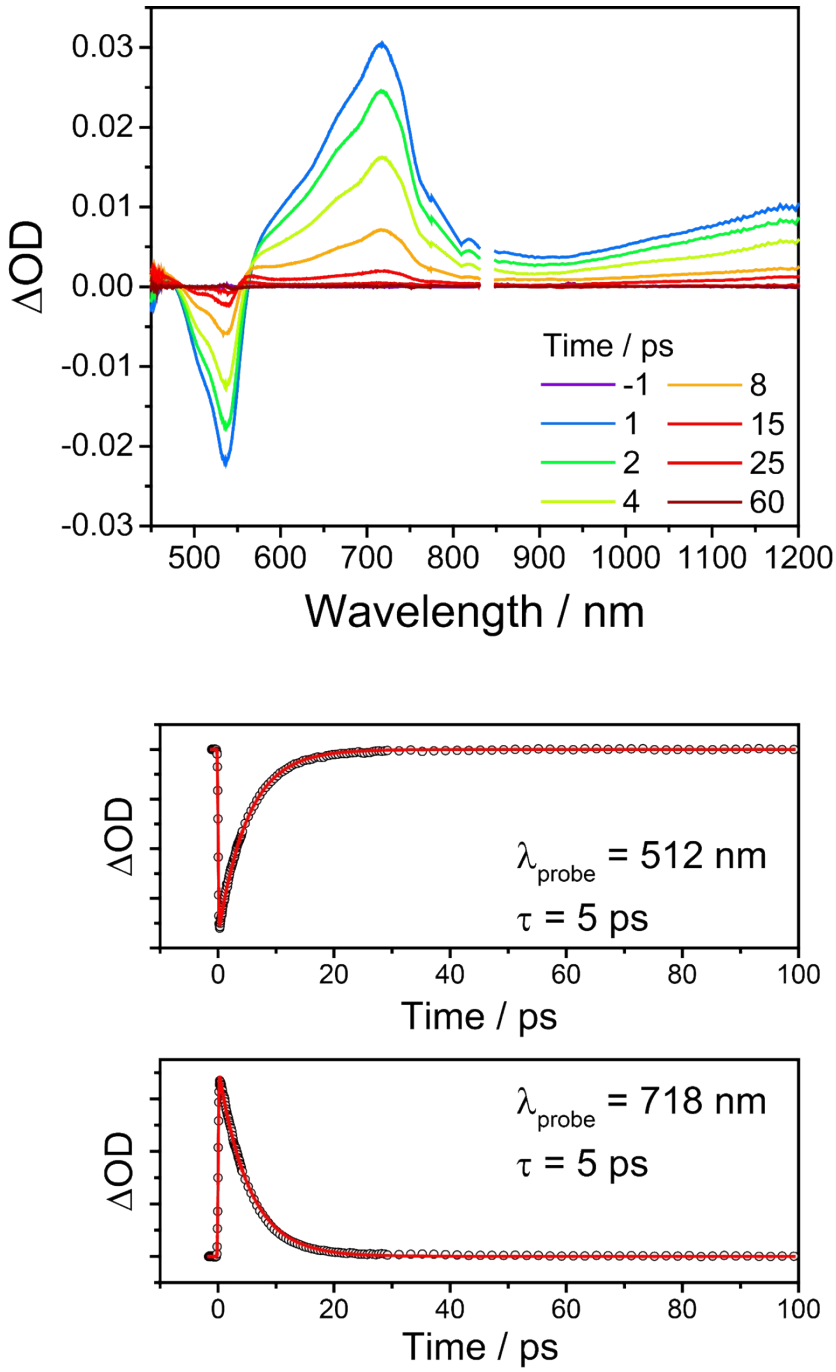

Figure S9-1. TA spectra (top) and decay profiles (bottom) of **8b** in CH_2Cl_2 with photoexcitation at 530 nm.

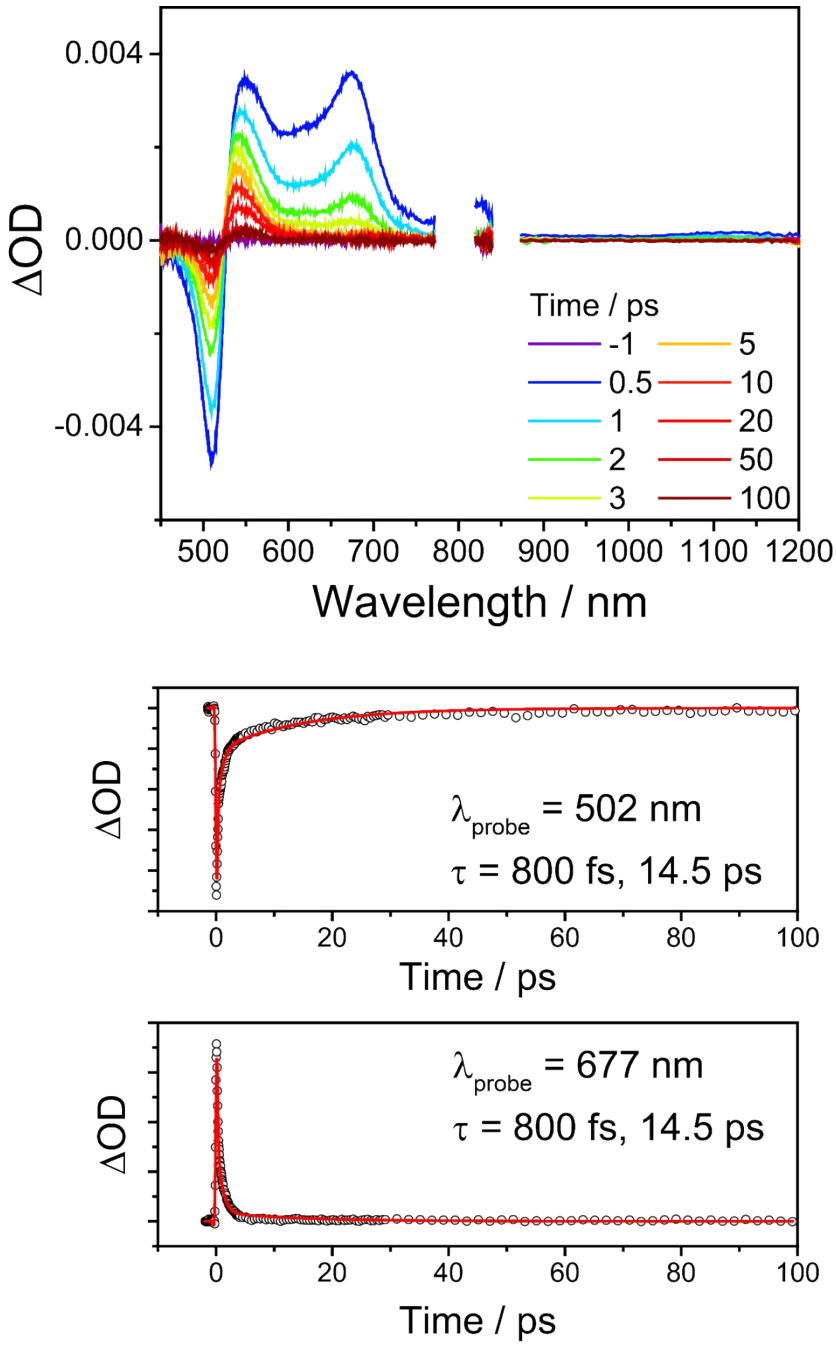

Figure S9-2. TA spectra (top) and decay profiles (bottom) of **10b** in CH_2Cl_2/pyridine with photoexcitation at 510 nm.

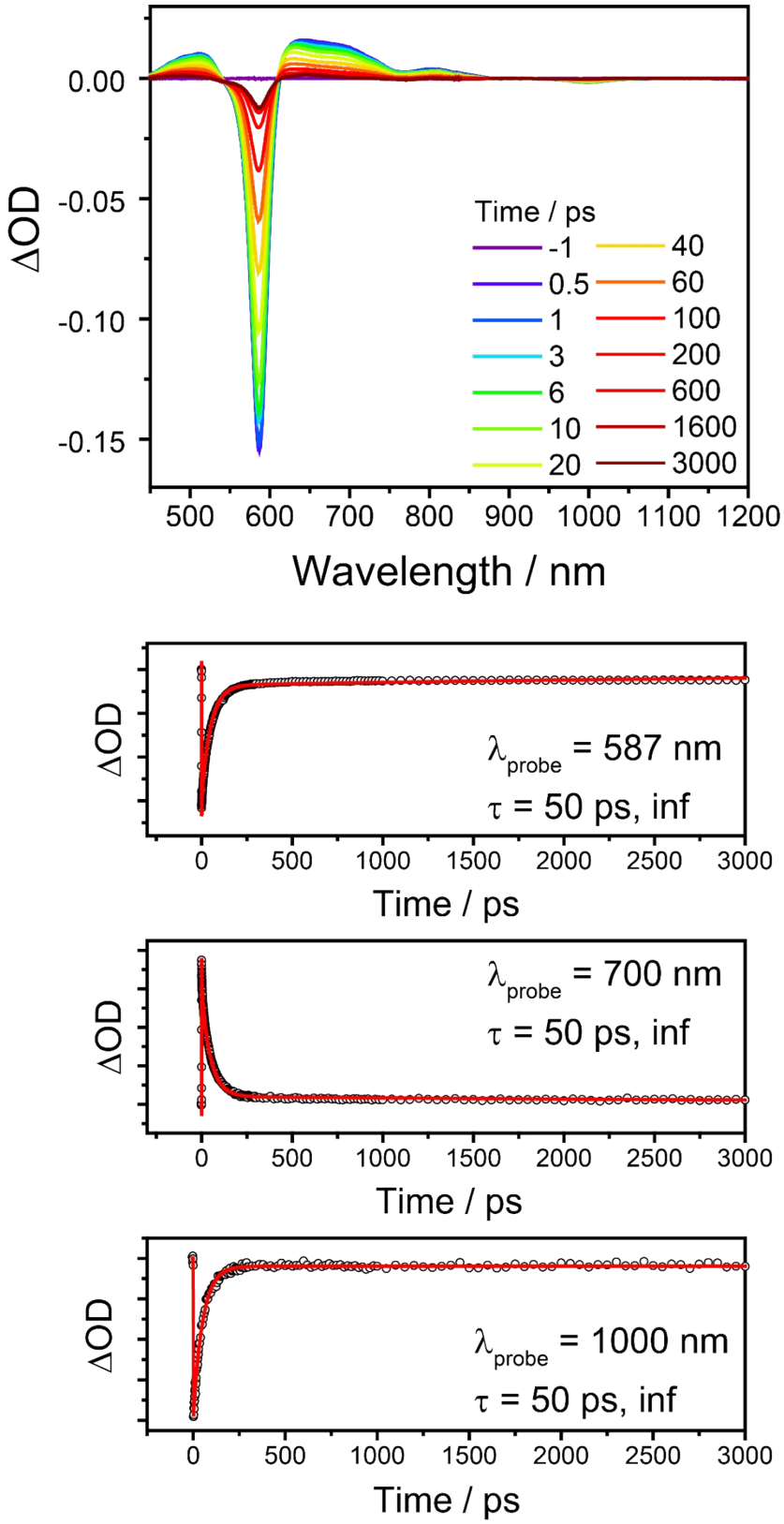

Figure S9-3. TA spectra (top) and decay profiles (bottom) of **11b** in CH_2Cl_2/pyridine with photoexcitation at 590 nm.

10. Supporting References

[S1] SHELXS-2013/1, SHELXT-2014/5, and SHELXL-2014/7, programs for refinement of crystal structures from diffraction data, University of Goettingen, Goettingen (Germany): a) G. Sheldrick and T. Schneider, *Methods Enzymol.*, 1997, **277**, 319; b) G. M. Sheldrick, *Acta Cryst.*, 2008, **A64**, 112; c) G. M. Sheldrick, *Acta Cryst.*, 2015, **C71**, 3.

[S2] Gaussian 16, Revision A.03, M. J. Frisch, G. W. Trucks, H. B. Schlegel, G. E. Scuseria, M. A. Robb, J. R. Cheeseman, G. Scalmani, V. Barone, G. A. Petersson, H. Nakatsuji, X. Li, M. Caricato, A. V. Marenich, J. Bloino, B. G. Janesko, R. Gomperts, B. Mennucci, H. P. Hratchian, J. V. Ortiz, A. F. Izmaylov, J. L. Sonnenberg, D. Williams-Young, F. Ding, F. Lipparini, F. Egidi, J. Goings, B. Peng, A. Petrone, T. Henderson, D. Ranasinghe, V. G. Zakrzewski, J. Gao, N. Rega, G. Zheng, W. Liang, M. Hada, M. Ehara, K. Toyota, R. Fukuda, J. Hasegawa, M. Ishida, T. Nakajima, Y. Honda, O. Kitao, H. Nakai, T. Vreven, K. Throssell, J. A. Montgomery, Jr., J. E. Peralta, F. Ogliaro, M. J. Bearpark, J. J. Heyd, E. N. Brothers, K. N. Kudin, V. N. Staroverov, T. A. Keith, R. Kobayashi, J. Normand, K. Raghavachari, A. P. Rendell, J. C. Burant, S. S. Iyengar, J. Tomasi, M. Cossi, J. M. Millam, M. Klene, C. Adamo, R. Cammi, J. W. Ochterski, R. L. Martin, K. Morokuma, O. Farkas, J. B. Foresman and D. J. Fox, Gaussian, Inc., Wallingford CT, 2016.

[S3] a) A. D. Becke, *J. Chem. Phys.*, 1993, **98**, 1372; b) C. Lee, W. Yang and R. G. Parr, *Phys. Rev. B*, 1988, **37**, 785.

[S4] a) D. Geuenich, K. Hess, F. Köhler and R. Herges, *Chem. Rev.*, 2005, **105**, 3758; b) R. Herges and D. Geuenich, *J. Phys. Chem. A*, 2001, **105**, 3214; c) R. Herges, *Chem. Rev.*, 2006, **106**, 4820.

[S5] Y. Zhang, J. Oh, K. Wang, C. Chen, W. Cao, K. H. Park, D. Kim and J. Jiang, *Chem. Eur. J.*, 2016, **22**, 4492.